Particle Accelerators and
High-Voltage Machines
(UC-28)

ANL--85-69

DE86 002540

ARGONNE NATIONAL LABORATORY
9700 South Cass Avenue
Argonne, Illinois 60439

AN OVERVIEW OF THE CHARACTERISTICS OF THE 6-GeV SYNCHROTRON RADIATION: A PRELIMINARY GUIDE FOR USERS

by

G. K. Shenoy and P. J. Viccaro

Materials Science and Technology Division

October 1985

TABLE OF CONTENTS

LIST OF FIGURES

LIST OF TABLES

AN OVERVIEW OF THE CHARACTERISTICS OF THE 6-GeV SYNCHROTRON RADIATION: A PRELIMINARY GUIDE FOR USERS

G. K. Shenoy and P. J. Viccaro

ABSTRACT

In this document we present the characteristics of the electromagnetic radiation from various types of sources on a 6-GeV storage ring. The sources include bending magnets, undulators and wigglers. The characteristics are compared with those of other synchrotron sources when operated at their design specifications. The influence of positron beam size on the brilliance is discussed, along with the power distribution from these sources. The goal of this document is to provide users with enough information on the behavior of radiation from a 6-GeV storage ring so that a dialogue can be established with the accelerator physicists and engineers to achieve an optimal design.

I. PURPOSE OF THIS DOCUMENT

During the past 12 months, accelerator physicists, engineers and users have been involved in the process of designing a national 6-GeV synchrotron source. Numerous workshops have been held and more are planned on various aspects of the 6-GeV synchrotron activity. We anticipate much closer interactions between the user community and the 6-GeV designers in the next few months. To facilitate these interactions, we felt the need to produce a document which would describe in some detail the characteristics of the 6-GeV synchrotron radiation. This preliminary report is intended to fulfill this goal, at least partially. All the calculations presented here are based on the so-called Model Storage Ring [1] for 6-GeV operation of a synchrotron source.

The past experience of the users at existing synchrotron sources should be used as an index of comparison with the planned 6-GeV source. Hence at many places in this document, we have provided the radiation characteristics of the presently operating sources and compared them with those of the 6-GeV source. In calculating these characteristics we have used the information available to us from the published or unpublished literature. These parameters may not exactly correspond to the operating parameters.

In some of our discussion, we will focus on specific scientific applications of the source. This is done intentionally to familiarize accelerator physicists and engineers with the users' jargon. Some of our discussions are drawn from our earlier Argonne National Laboratory Light Source (LS) design documents and presented in a revised form to include newer thoughts. We will provide more illustrations than words to convey the facts on radiation characteristics of the 6-GeV storage ring.

No attempt is made to provide a comprehensive bibliography for this document. A few references of direct concern are cited.

II. CHOICE OF 6-GeV STORAGE RING PARAMETERS

The general characteristics of the radiation from a 6-GeV source, based on broad requirements of the user community, were outlined in a workshop held in Ames, Iowa during October 1984. Since then accelerator physicists and engineers from various institutions including ANL, BNL, CESR/CHESS, ESRF, LBL, SLAC and SSRL have met and refined the 6-GeV storage ring parameters. The currently accepted set of parameters of importance to the users are presented in Table 1. Some of the discussion related to the choice of these parameters is in the Report of the Machine Workshop on the 6-GeV Synchrotron Radiation Source, March 28-30, 1985 (copies are available from the U.S. Department of Energy, Tel. (301) 353-3426).

III. SOURCE SIZE AND BRILLIANCE

For users of this low-emittance lattice, the source size is of utmost importance. The size of the source is a function of the emittance of the lattice and the values of the amplitude function β (betatron tune). The values of β are determined by the focusing properties of the magnetic lattice and will be different in various sections of the ring. The emittances in the horizontal (ε_x) and vertical (ε_y) directions are given by

$$\varepsilon_x = \frac{\varepsilon_o}{1 + k^2} ,$$

$$\varepsilon_y = \frac{\varepsilon_o k^2}{1 + k^2} ,$$

where $\varepsilon_o = 8\text{x}10^{-9}$ m•rad is the expected emittance of the 6-GeV lattice. With positron beam coupling in the x-y plane defined by $k^2 = 0.1$ (for the lattice), we obtain

$$\varepsilon_x = 7.3\text{x}10^{-9} \text{ m•rad}$$

and

$$\varepsilon_y = 7.3\text{x}10^{-10} \text{ m•rad.}$$

In terms of the betatron functions β_x and β_y, the source size (assuming a Gaussian shape) is given by the following:

Horizontal beam size $\sigma_x = \sqrt{\varepsilon_x \beta_x}$,

Vertical beam size $\sigma_y = \sqrt{\varepsilon_y \beta_y}$,

Table 1. Parameters of Model Storage Ring for a 6-Gev Operation

Ring Energy, E_R (GeV)	6±10%
Beam Current, I (mA)	100
Number of Stored Positrons	1.6×10^{12}
Magnet Bending Radius, ρ (m)	30.0
Bending Field (T)	0.67 (6 GeV)
Ring Circumference (m)	800
Symmetric Periods	16
Natural Emittance, ε_o (m•rad)	8.0×10^{-9}
xy Coupling Parameter, k^2	0.1
Beam Height from Floor (m)	1.5
Bending Magnet Sources	32
Insertion Devices (maximum)	28
Free Lengths for Insertion Devices (m)	6.0
Revolution Period (μsec)	2.67
Ring Damping Time (msec)	4.2
RF Frequency (MHz)	350.76
RF Power Available (MW)	1.0
Beam Lifetime (h)	8

Horizontal beam divergence $\sigma_x' = \sqrt{\epsilon_x/\beta_x}$,

Vertical beam divergence $\sigma_y' = \sqrt{\epsilon_y/\beta_y}$

In Table 2, we present the beam size and divergence in various parts of the lattice in the absence of any insertions.

The spectral brilliance, B, is defined as the photon flux, F, per unit area of horizontal and vertical phase space. The units of flux are photons/sec/0.1%BW/mrad θ. The phase space volume is obtained by convoluting the Gaussian distributions describing the source and the radiation field. If Σ_i and Σ_i' (i = x,y) are the beam size and divergence, then the brilliance of the source is given by

$$B(x,y,\theta,\phi) = \frac{F\, e^{-\frac{1}{2}\left(\frac{x^2}{\Sigma_x^2} + \frac{y^2}{\Sigma_y^2} + \frac{\theta^2}{\Sigma_x'^2} + \frac{\phi^2}{\Sigma_y'^2}\right)}}{(2\pi)^2\, \Sigma_x \Sigma_y \Sigma_x' \Sigma_y'} .$$

Here the denominator represents the phase space volume and θ and ϕ are the angular coordinates of the beam along the x and y directions. Typical units of B are photons/sec/0.1%BW/mrad^2/mm^2. Note that many authors use the word brightness for what we have called brilliance.

In a straight section containing an undulator, the effective divergence and the size, Σ_i' and Σ_i (i=x,y), of the source are dependent on the apparent source size of the radiation field σ_R and the opening angle σ_R' of the radiation. σ_R and σ_R' are functions of the radiation wavelength λ and undulator length L, and they include depth of field and/or diffraction effects. Recently, Kwang-Je Kim has shown (SRI-85) that the effective source size in an undulator is given by

$$\Sigma_x = (\sigma_x^2 + \sigma_R^2)^{1/2} \quad ; \quad \Sigma_y = (\sigma_y^2 + \sigma_R^2)^{1/2}$$

and the effective divergence by

$$\Sigma_x' = (\sigma_x'^2 + \sigma_R'^2)^{1/2} \quad ; \quad \Sigma_y' = (\sigma_y'^2 + \sigma_R'^2)^{1/2}$$

with $\sigma_R = \frac{1}{4\pi}\sqrt{\lambda L}$; $\sigma_R' = \sqrt{\frac{\lambda}{L}}$.

The brilliance in the case of an undulator will be achieved through a superposition of source phase spaces along the length of the device. Thus the average brilliance in this case (averaged over the length of the device) is obtained by dividing the flux by $4\pi^2 \Sigma_x \Sigma_y \Sigma_x' \Sigma_y'$ as shown above.

It is clear that the effective phase space volume is dependent on the betatron functions β_x, β_y for a device of fixed length in a storage ring. Thus we can maximize the brilliance (reducing the phase space volume) by varying β_x

and β_y. We have demonstrated the brilliance optimization for our 6-GeV lattice in Fig. 1, where $(\Sigma_i \Sigma_i'/\sigma_i \sigma_i') - 1$ is plotted as a function of $\beta_i (i=x,y)$. The phase space minimum occurs at $\beta_x = \beta_y = L/2$, although the phase space volume is rather insensitive to β_x and β_y. The dependence of the effective source size on photon energy is flat for short-wavelength radiation and becomes significant only for photon energies below about 1 keV for our lattice.

In this document we will use the β-values given in Table 2. The actual effective source sizes and divergences, $\Sigma_x, \Sigma_y, \Sigma_x', \Sigma_y'$, will be determined by β_x and β_y. In this case, $\Sigma_x \sim \sigma_x$, $\Sigma_y \sim \sigma_y$.

The source dimensions in the case of wigglers are more complex because of the multiple incoherent source points along the wiggler length. The β_x and β_y given in Table 2 will be close to the L/2 criterion discussed above. Furthermore, for the 6-GeV low-emittance lattice, in the normal direction of observation (θ=0), the depth-of-field effects are not significant. A detailed analysis with respect to each of the devices will be needed.

TABLE 2. 6-GeV Source Size in Different Parts of the Lattice

	Bending Magnet	Undulator	Wiggler
β_x (m)	0.92	22.5	1.37
β_y (m)	24.4	13.15	1.24
σ_x (μ)	82	405	100
σ_y (μm)	133	98	30
σ_x' (μrad)	89	18	73
σ_y' (μrad)	5	7	24

IV. BENDING MAGNET SOURCES [2]

The primary purpose of the 6-GeV synchrotron is to provide insertion-device-based sources. However, it can also deliver bending-magnet (BM) radiation in 32 ports. It is anticipated that in view of excessive requests for time on the hard x-ray ports available on various synchrotrons in the U.S., the 6-GeV synchrotron will be in demand for its BM radiation.

Also, there are many situations, such as in protein crystallography, where high-energy radiation is extremely useful, but the sample cannot take the heat loads from an insertion device source. The 6-GeV BM radiation is well suited to such situations. Furthermore, the small source size (Table 2)

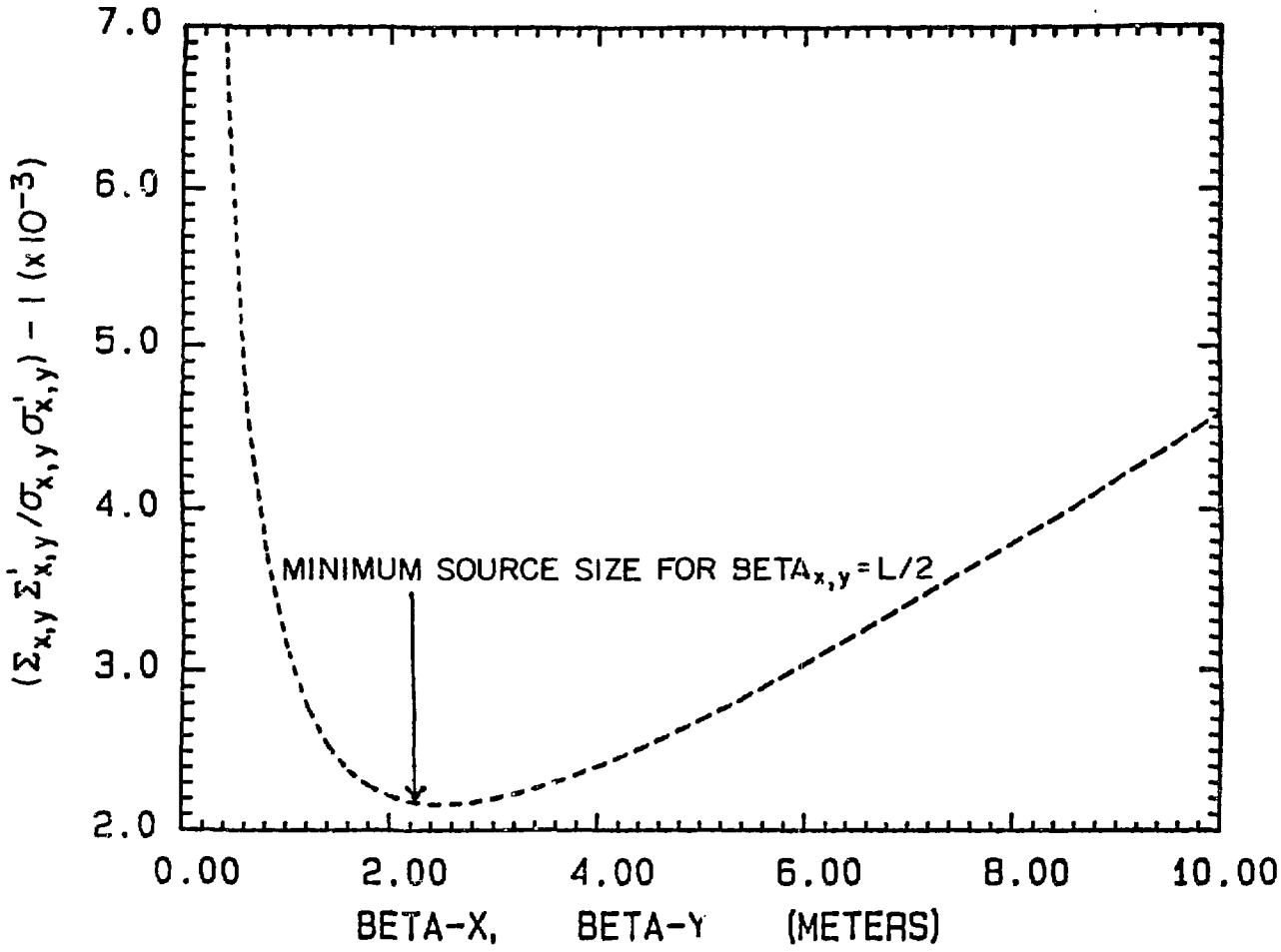

Fig. 1. Plot of $\Sigma_i\Sigma_i'/\sigma_i\sigma_i' - 1$ vs β_i (i=x,y) for a 5-m-long insertion device on a 6-GeV storage ring.

would be useful for improving even the conventional measurements that are now being made by use of BM radiation. An example is structural investigations on single crystals of materials which are only available in sizes of 10-100 μm.

A. Power Distributions

In the present lattice with 64 BMs, the radiation from each bend will cover 98.17 mrad, as shown in Fig. 2. The vertical opening angle 2ψ of this radiation sheet is approximately $2/\gamma$.

$$2\psi \simeq 2/\gamma \simeq 0.2 \text{ mrad};$$

$$\gamma = 1957\ E_R\ (\text{GeV}) = 11742,$$

where E_R is the positron energy. The length of the trajectory of the positron through each bend is 2.94 m.

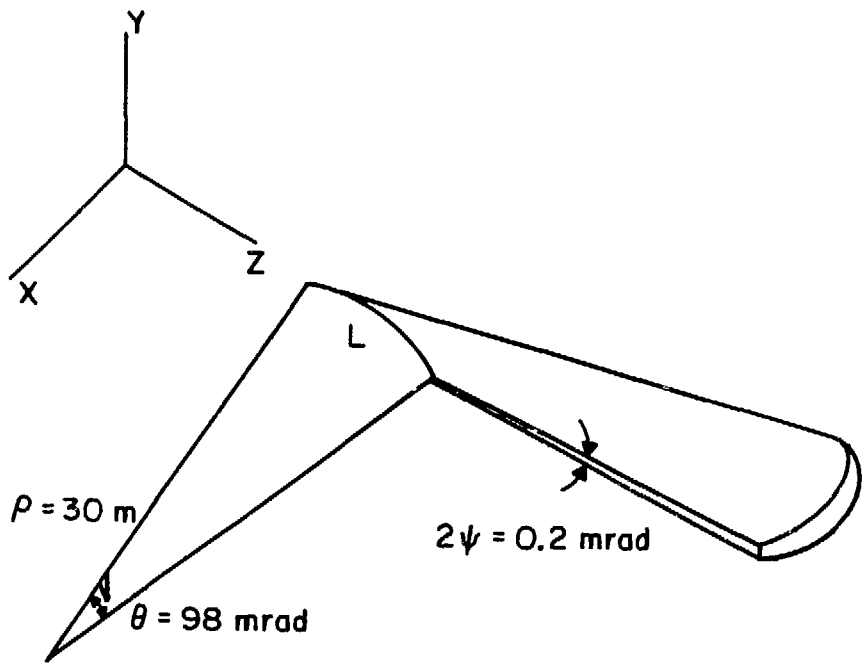

Fig. 2. Coordinate system used for defining the properties of radiation from a 6-GeV bending magnet.

The radiation from a BM source has a uniform distribution in the horizontal (xz) plane. In the vertical direction, the brightness is a function of angle ψ, and is given by

$$\text{BR(ph/sec/mrad } \theta\text{/mrad } \psi\text{/0.1\%BW)} = 1.32\text{x}10^{10} I(\text{mA}) E_R^2(\text{keV}^2)/E_c^2(\text{keV}^2) F(\gamma\psi) \quad (1)$$

where

$$F(\gamma\psi) = (\gamma\psi)^2[1 + (\gamma\psi)^2]K_{1/3}^2(\zeta) + [1 + (\gamma\psi)^2]^2K_{2/3}^2(\zeta) \quad (2)$$

and

$$\zeta = \left(\frac{E}{2E_c}\right)[1 + (\gamma\psi)^2]^{3/2}, \quad (3)$$

where E is the photon energy in keV. The critical energy E_c is given by

$$E_c(\text{keV}) = 0.665\ E_R^2(\text{GeV}^2)B(T)\ , \quad (4)$$

where B is the BM field and $K_{1/3}$ and $K_{2/3}$ are Bessel functions of fractional order. For our ring, E_c = 16 keV (0.78 Å).

In Fig. 3, we present Eq. (1) as a function of ψ for various values of E. We observe that at low energies (< 2 keV), the radiation spread is well above the so-called opening angle of $2/\gamma$. The radiation with $E = E_c$ carries maximum brightness. In Fig. 4, we have contrasted the behavior of the NSLS ring. We wish to point out an interesting possibility for obtaining soft x-rays (< 2 keV) from the 6-GeV BM source. One could use a cooled in-plane mask to shield the high-energy radiation and collect the soft x-rays by use of appropriate optics based on metallic multilayers. The brightness in this part of the distribution ($\psi > 2/\gamma$) is adequate to obtain useful soft x-ray radiation, and is comparable to that from NSLS (500 mA).

The two terms in Eq. (2) correspond to polarizations perpendicular and parallel to the plane of the positron orbit (xz plane), respectively. The BM radiation is almost linearly polarized in the plane of the orbit at $\psi = 0$. With increasing ψ, the perpendicular polarization gradually increases at the cost of polarization parallel to the xz plane. These two components of polarization are phase correlated, and hence one can realize elliptically polarized radiation as ψ increases from $\psi = 0$. The helicity of polarization is opposite above and below the orbit plane (xz). In Fig. 5 we present the degree of linear polarization for radiation of various energies as a function of ψ. The spatial distribution of polarization can be very profitably used in experiments requiring elliptically polarized radiation. The linear polarization of 1.0 is true for a single positron trajectory. For a beam with non-zero divergence, the radiation at $\psi = 0$ with E_c = 16 keV will have $P_\perp/P_\parallel \approx 31\times10^{-6}\sigma_z^2$ (μrad^2). This ratio is less than 0.1% in our case provided the radiation is collected in a 5-μrad cone. Brightness in the polarization components along x($P_\parallel$) and y($P_\perp$) directions as a function of ψ for 2-keV BM radiation is shown in Fig. 6. The degree of circular polarization, $2(P_\parallel P_\perp)^{1/2}/(P_\parallel + P_\perp)$, is about 0.9 at 0.13 mrad.

Integrating Eq. (1) over all the energy provides us with the ψ dependence of total power:

$$\frac{\partial P}{\partial \psi} = 1.24\times10^{-2}\ E_R^4(\text{GeV}^4)B(T)I(\text{mA})F(\gamma\psi)\quad \text{W/mrad}\ \theta/\text{mrad}\ \psi, \quad (5)$$

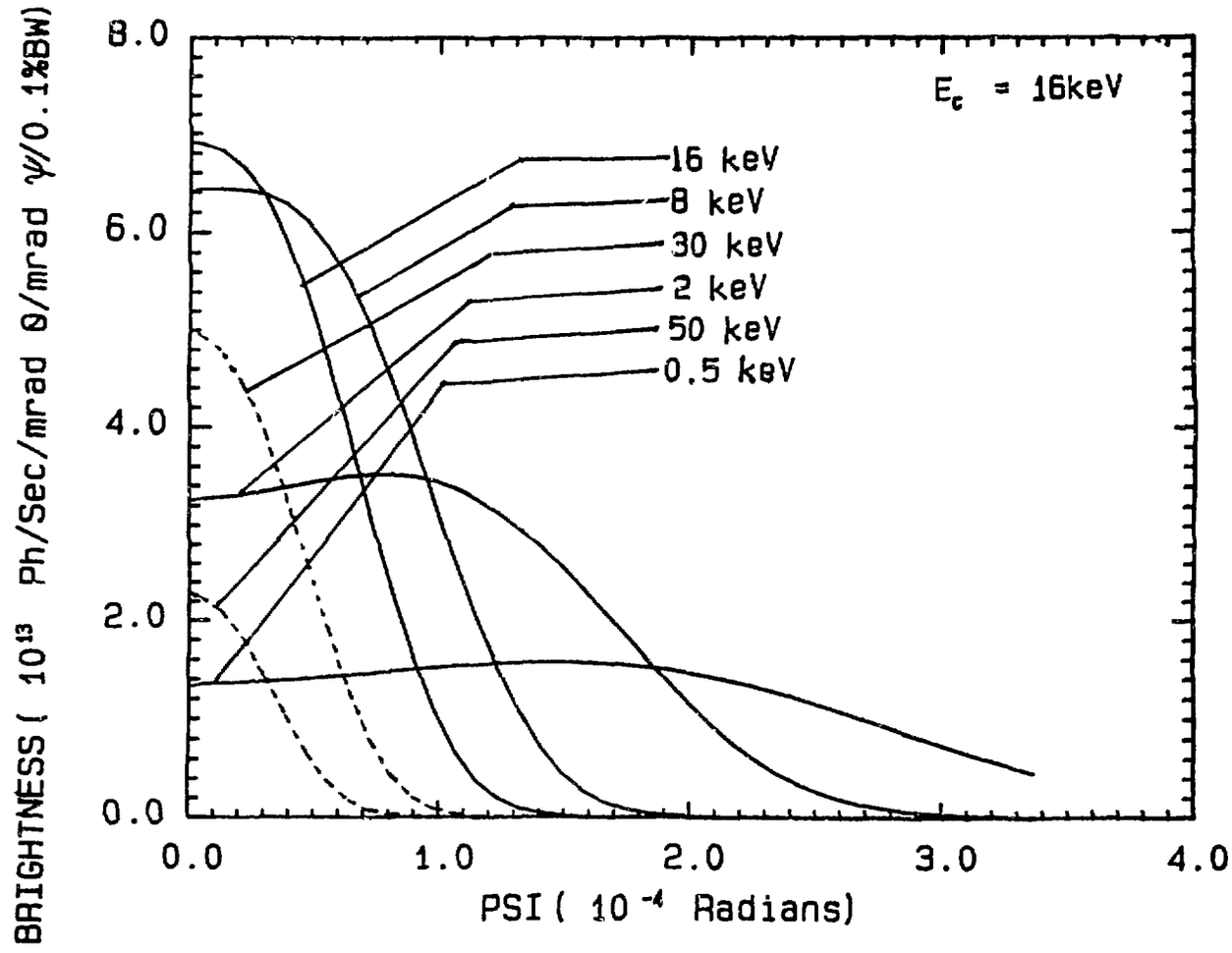

Fig. 3. Brightness of bending-magnet radiation from a 6-GeV storage ring (100 mA) as a function of vertical opening angle ψ for various photon energies.

Fig. 4. Same as Fig. 3 for the NSLS storage ring (2.5 GeV, 500 mA).

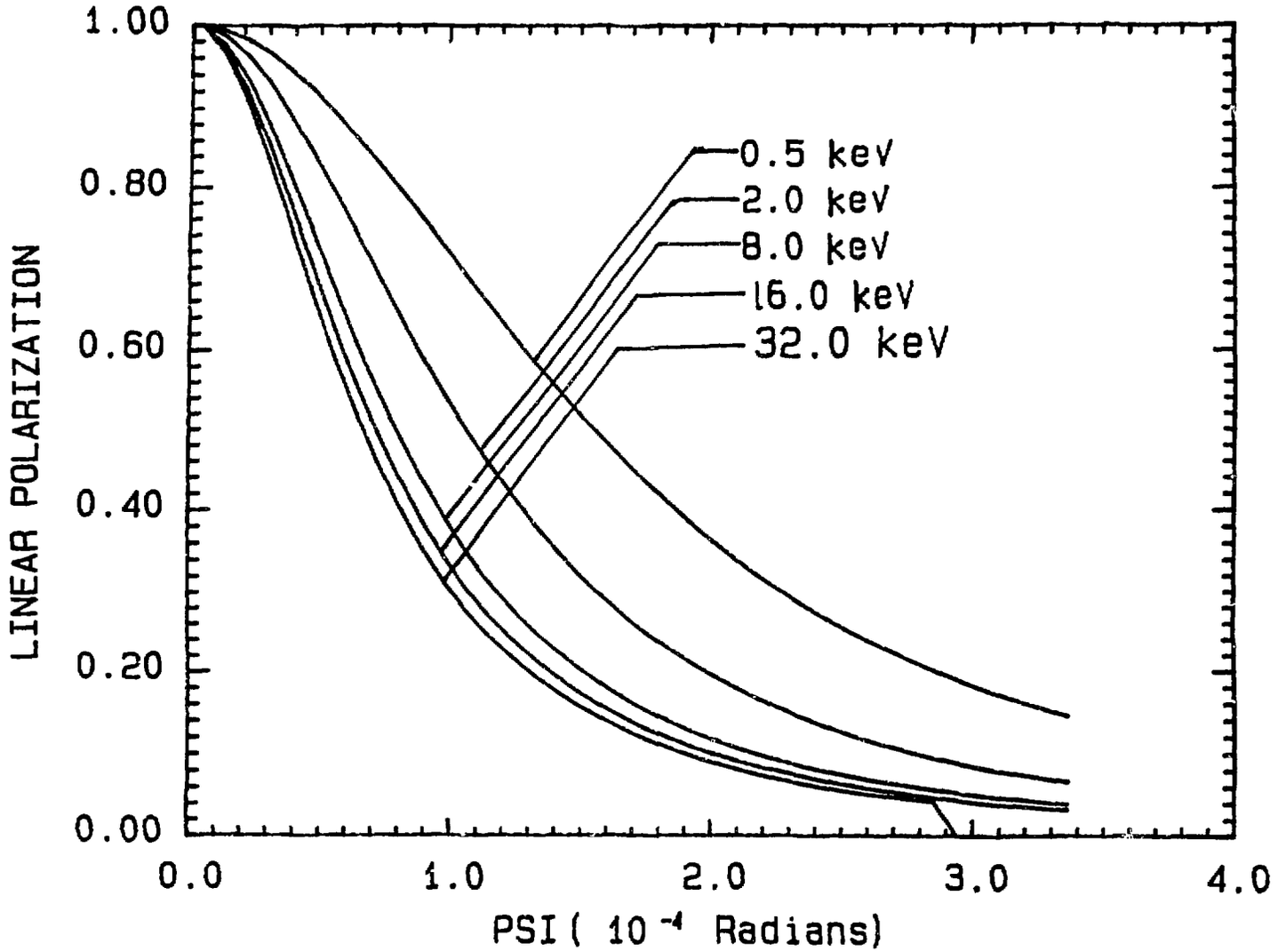

Fig. 5. Degree of linear polarization (based on single-orbit theory) as a function of vertical opening angle ψ for various photon energies from a 6-GeV bending magnet (100 mA).

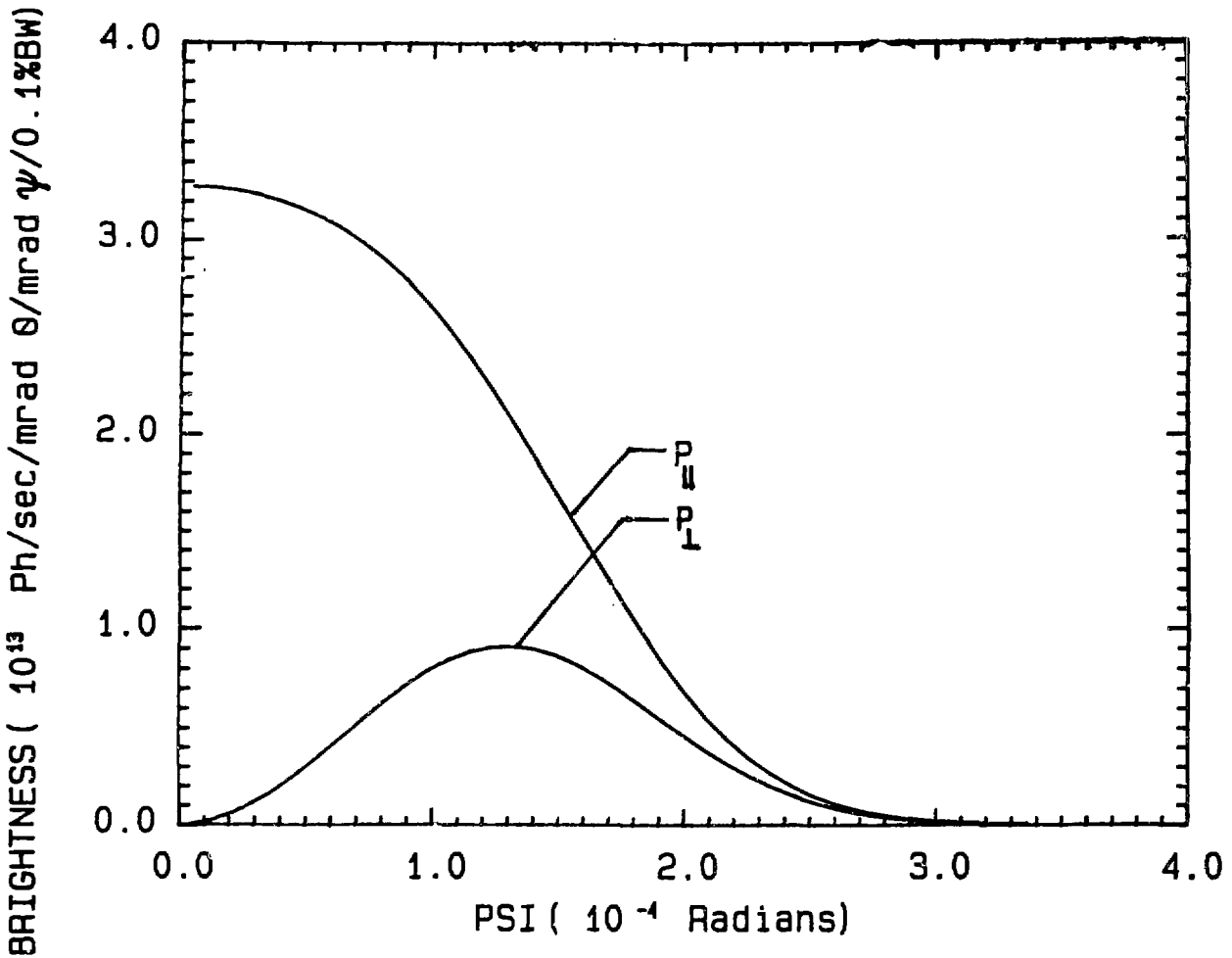

Fig. 6. Brightness of polarization components parallel and perpendicular to the orbital plane as a function of vertical opening angle ψ for 2-keV radiation from a 6-GeV bending magnet (100 mA).

where

$$F(\gamma\psi) = (1 + \gamma^2\psi^2)^{-5/2} [7 + 5(\gamma^2\psi^2)/(1 + \gamma^2\psi^2)]/16. \quad (6)$$

The distribution is given in Fig. 7, which shows the total power as a rectangle of width equal to $2x0.77/\gamma$. The power at $\psi = 0$ is

$$P(\psi = 0) = 0.54x10^{-2} E_R^4 (GeV^4) B(T) I(mA) \text{ W/mrad } \theta/\text{mrad } \psi. \quad (7)$$

For our ring, $P(\psi=0) = 470$ W/mrad θ/mrad ψ.

By integrating for all the photon energies and ψ (Eq. (1)) and θ, we obtain the total radiated power from a BM:

$$P(W) = 1.263 B^2(T^2) E_R^2 (GeV^2) I(mA) L(m). \quad (8)$$

For our lattice, P = 6021 W. Thus, per mrad θ, the radiation provides 60 W of total power over all ψ. It is important to recognize that this is the total power, whereas the peak power (at $\psi = 0$) is 470 W. This is contrasted with the NSLS in Table 3. Although the total power of the 6-GeV storage ring is only 1.5 times that of the NSLS, the peak power is greater by a factor of 3.7. This fact is important in designing the procedures for handling the heat load from the first optical elements.

There are 64 such dipoles (only 32 accessible to users), and hence the ring radiates 385 kW of total power. At 6.6-GeV (6+10%) operation, total radiated power will be 562 kW.

TABLE 3. Power Delivered by BM Sources

	6-GeV Source	NSLS
Energy (GeV)	6	2.5
Current (mA)	100	500
Peak power (W/mrad θ)	470	128
Average power (W/mrad θ)	60	40
Critical energy, E_c (keV)	16	5
2ψ (mrad) = $2/\gamma$	0.17	0.41

B. Flux, Brightness and Brilliance:

In many experiments, the total number of photons or flux (expressed in photons/sec/0.1%BW/mrad θ) is of importance. Presently operating synchrotron sources provide large fluxes and meet such needs.

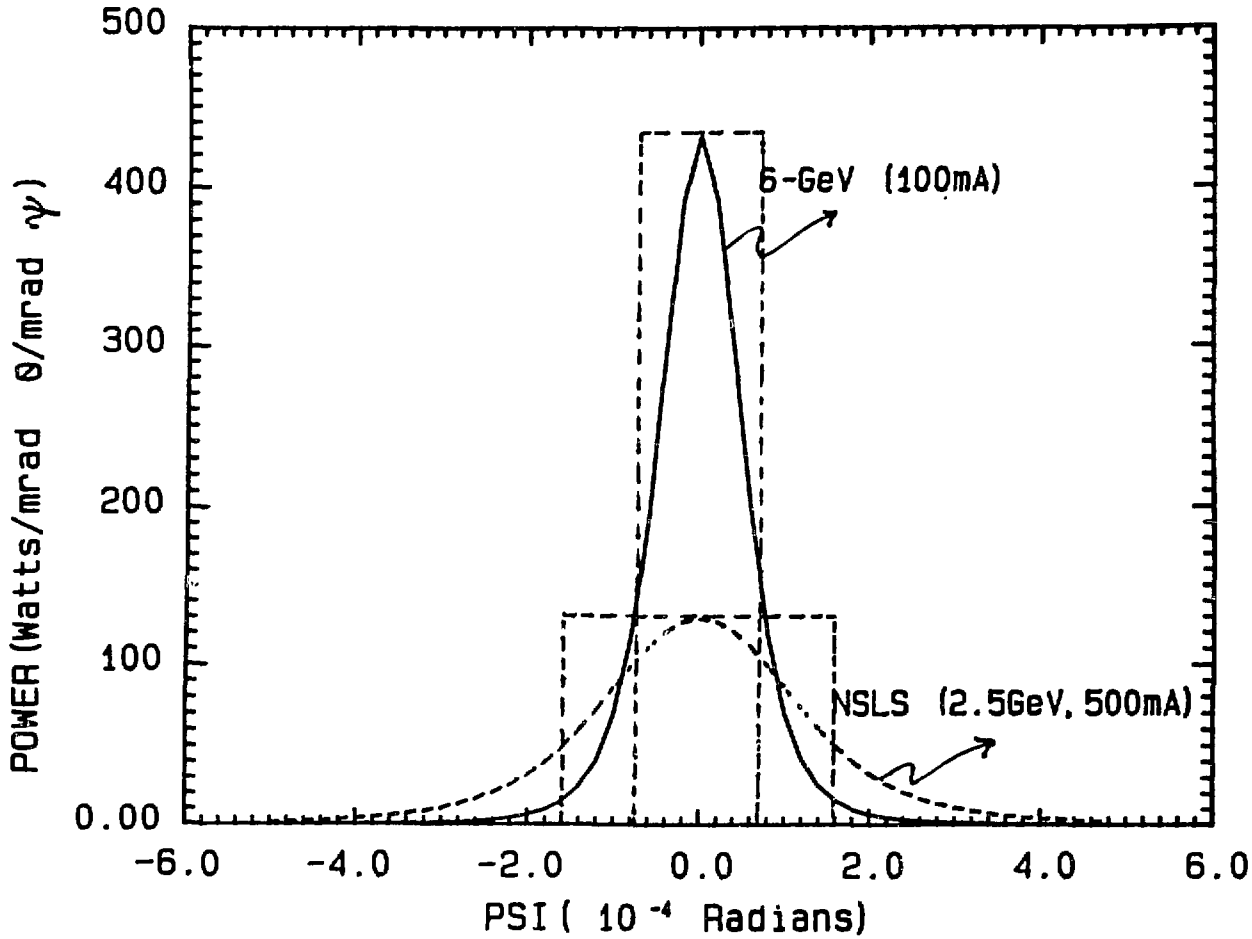

Fig. 7. Power distribution of radiation from a bending magnet on a 6-GeV storage ring and NSLS as a function of vertical opening angle ψ.

In situations where the beam need not be focused on the sample, the spectral brightness (expressed in photons/sec/0.1%BW/mrad^2) is of importance. High brightness is achieved if the beam has small divergence (σ_x' and σ_y' or Σ_x' and Σ_y').

If the source can be focused (by using appropriate optics) on the sample, then having a small source size is of utmost importance. In such a case we define spectral brilliance (in photons/sec/0.1%BW/mrad^2/mm^2), which can be increased by making both the source size (σ_x and σ_y or Σ_x and Σ_y) and the source divergence as small as possible. As we have pointed out earlier, the 6-GeV ring is designed with low emittance (ε_x and ε_y) precisely with this in mind.

We have already seen that the source emittance and betatron functions determine the values of σ_x, σ_y, σ_x' and σ_y' for the BM sources (Σ_x,Σ_y,Σ_x' and Σ_y' for the insertion sources).

In Figs. 8, 9 and 10 we have compared the flux, brightness and central brilliance from BMs of the 6-GeV source with various sources. The parameters used in arriving at these figures are presented in Table 4.

We observe that the BM radiation from the 6-GeV source has the highest brilliance over the whole spectral range, and the energy range extends to much higher values. The flux and brightness of the 6-GeV source dominates at energies over about 7 keV.

Table 4. Parameters of Various BM Sources

	6-GeV	ESRF	NSLS	SSRL	CHESS
E (GeV)	6.0	5.0	2.5	3.0	5.5
I (mA)	100	100	500	100	40
ρ (m)	30.0	20.0	6.8	12.7	32.0
B (T)	0.67	0.83	1.22	0.79	0.57
E_c (keV)	16.0	14.0	5.1	4.7	11.5
σ_x (mm)	0.082	0.092	0.3	2.0	1.44
σ_y (mm)	0.133	0.100	0.1	0.28	1.0

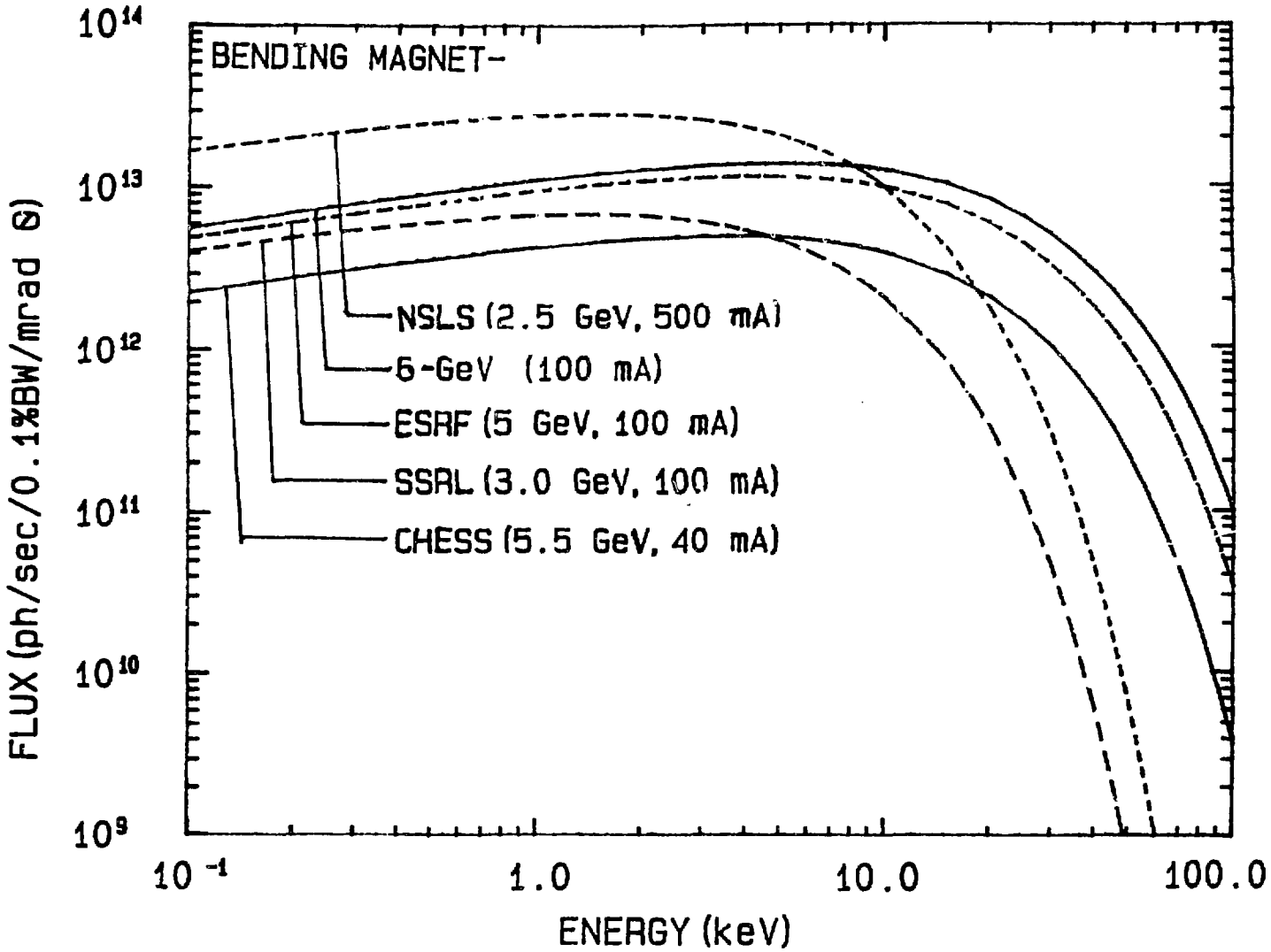

Fig. 8. Flux from a bending magnet on various synchrotron sources.

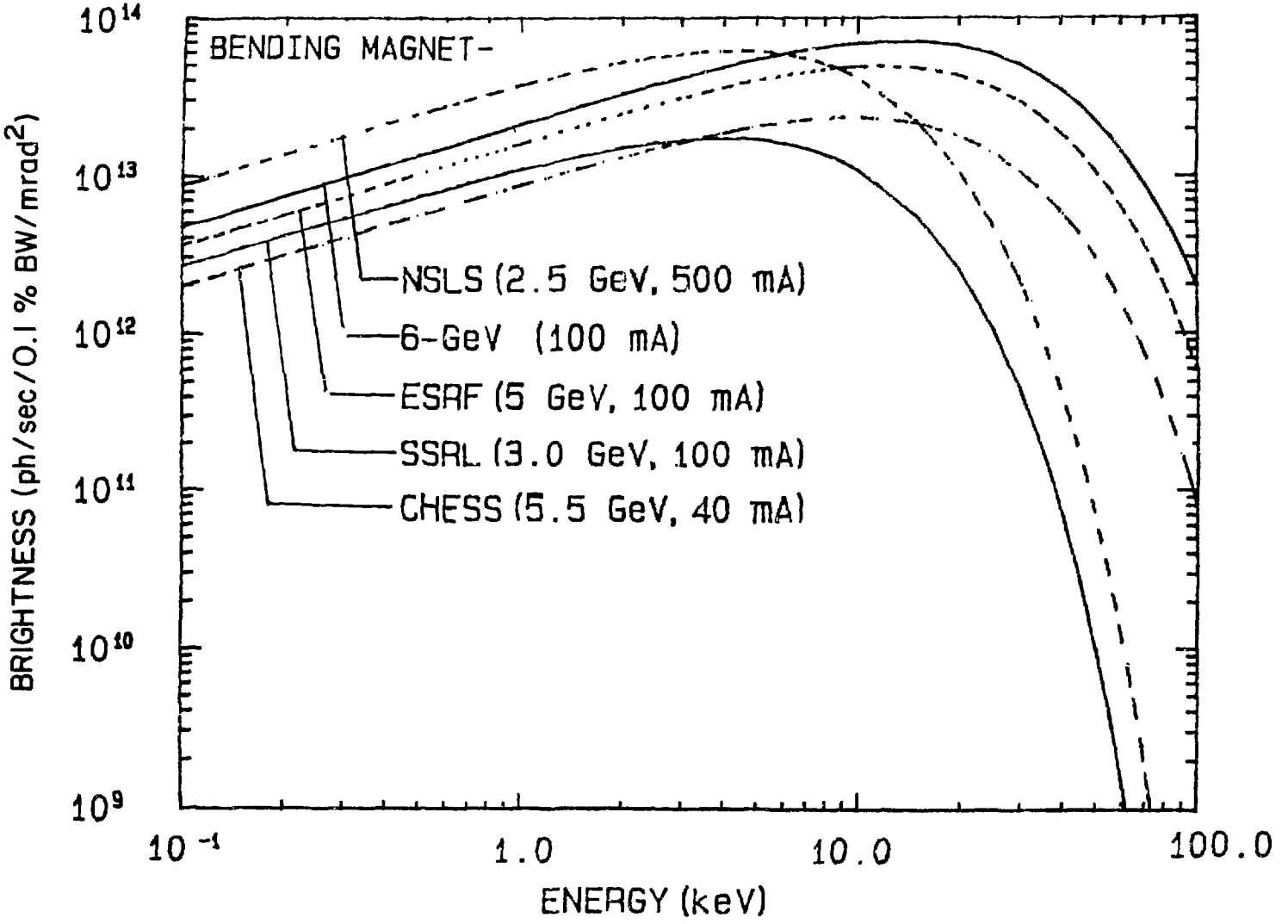

Fig. 9. Brightness of bending-magnet radiation from various synchrotron sources.

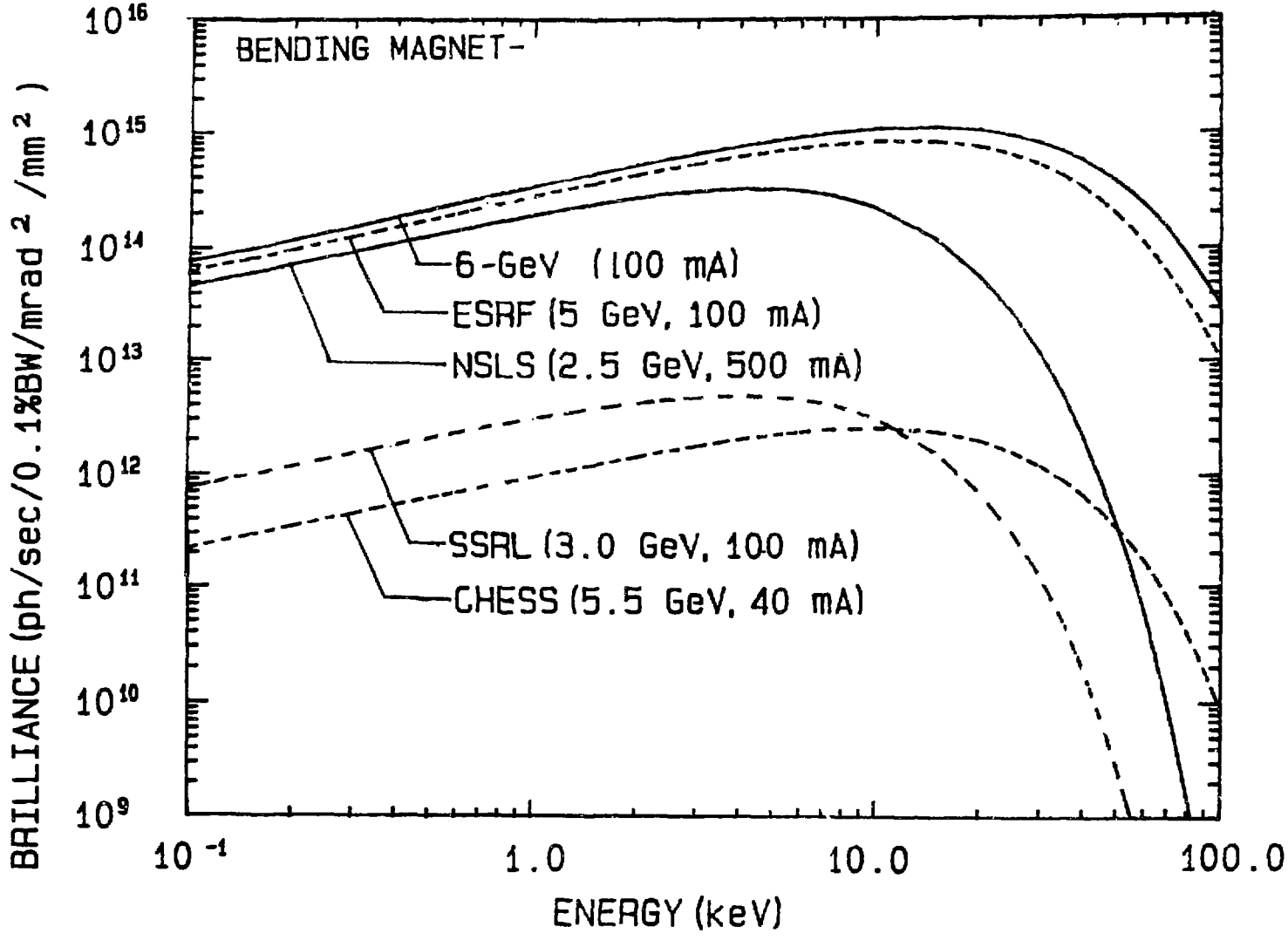

Fig. 10. Brilliance of bending-magnet radiation from various synchrotron sources.

V. UNDULATOR SOURCES

Undulator sources provide pseudomonochromatic radiation and their high brilliance has many uses, including the following:

- Ultrahigh-resolution inelastic scattering ($\delta E/E \sim 1\text{-}5\times10^{-7}$) to study, for example, phonon excitations.
- Intermediate-resolution inelastic scattering ($\delta E/E \sim 10^{-4}$) to study, for example, charge density waves.
- High-momentum-resolution scattering ($\Delta k \sim 10^{-4}$ Å^{-1}) to study, for example, surface diffraction and long-wavelength magnetic modulations.
- Small-angle scattering.
- High-resolution monochromatic topography.
- Elastic magnetic scattering.
- Nuclear resonant diffraction for coherent x-ray radiation.
- Anomalous scattering.
- Soft x-ray applications.
- X-ray microprobe and fluorescence analysis.

In designing undulators on a 6-GeV storage ring, one of the the primary considerations will be the power that such devices will deliver. The beam-line design must be capable of handling large powers. Specifically, in the front-end of a beam line we have masks (fixed and movable) followed by various optical components. Many thermal designs are now being developed to permit various components to handle a greater heat load than ever before possible. For example, designs for rotating optics and liquid-metal-cooled optics are being actively pursued in the MST division at ANL.

A conservative approach to power-handling problems is to go by our experience with devices operating on existing storage rings. The 54-pole wiggler on SPEAR is perhaps the hottest device operating today. The fixed and movable masks located 6.5 m from the source on Beam Line VI at SSRL are designed to handle 200 W/mm^2. These components are cooled with water only, with an efficient cooling design. The heat-load handling can be improved by a large factor with newer approaches. These considerations are most important in deciding the design of various undulators on a 6-GeV storage ring.

The other important considerations in an undulator design are related to the capability of permanent magnets and to the minimum permissible undulator gap. Within the framework of presently available magnet technology, these factors may impose some limitations in meeting all the user demands on the spectral range and brilliance or flux, as the case may be.

Finally, we will present a spectrum of undulators based on hybrid magnets that will cover most of the presently conceived user demands from under 0.5 keV to 21 keV at a 6-GeV storage ring. Typical plots of on-axis average spectral brilliance from a few undulators are also presented.

A. Undulator Power

Let us assume the undulator to be L meters long and to have N periods, each λ_o cm long. Then the total power radiated by the undulator on a storage ring with positrons of energy E_R and current I is given by

$$P(W) = 7.25\times10^{-3}\ E_R^{\ 2}(GeV^2)\ I(mA)\ N\ K^2/\lambda_o. \qquad (9)$$

The deflection parameter K is given by

$$K = \gamma\lambda/2\pi\rho,$$

where ρ_o is the radius of the positron trajectory. In practical units $K = 0.934\ B_o\lambda_o$ (B_o is the peak field in tesla and λ_o is the period in cm). One can also express

$$P(W) = 0.634\ E_R^{\ 2}\ (GeV^2)\ B_o^{\ 2}\ (T^2)\ I(mA)\ L(m). \qquad (10)$$

A typical value of B_o is 0.3 T, which for L = 5 m, I = 100 mA, and E_R = 6 GeV yields a total radiated power of 1027 W.

This power, when calculated per unit solid angle in the forward direction, is approximately 117 kW/mrad^2. Many experiments will demand 30- to 100-m-long beam lines. At 30 m, the forward-direction power density in this example is 130 W/mm^2 and this is less than the power density that can be handled by the 54-pole wiggler beam line at SSRL. The finite size of the source will reduce this power density by a factor of about 1.5.

From the above, it appears that there should be no serious difficulties in power handling by the beam line components. On the other hand, by the time the 6-GeV ring is operational, we are sure to encounter newer demands on devices, which may be longer in length (L) or have larger fields (B_o) (and smaller periods to keep $K < 1$), etc. These requirements will increase their power considerably, and will necessitate effective solutions for power handling, like the ones mentioned earlier.

B. Undulator Magnets and Gap

Presently, REC ($SmCo_5$) magnets or REC/vanadium permendur hybrid magnets are employed in undulators (Fig. 11). An alloy of Nd-Fe-B shows considerable promise with its capability to produce 20-30% larger fields than the hybrid magnets for the same geometrical configuration. Klauss Halbach (SRI-85) has presented a newer concept in magnet design which combines permanent magnets and electromagnets. These developments will lead to newer undulators capable of producing radiation suitable for experiments which are at present considered difficult or not yet conceived. For the present exercise, we will discuss well-documented hybrid magnets only. For the REC-based hybrid magnets made up of $SmCo_5$ blocks and vanadium permendur poletips, the dependence of the

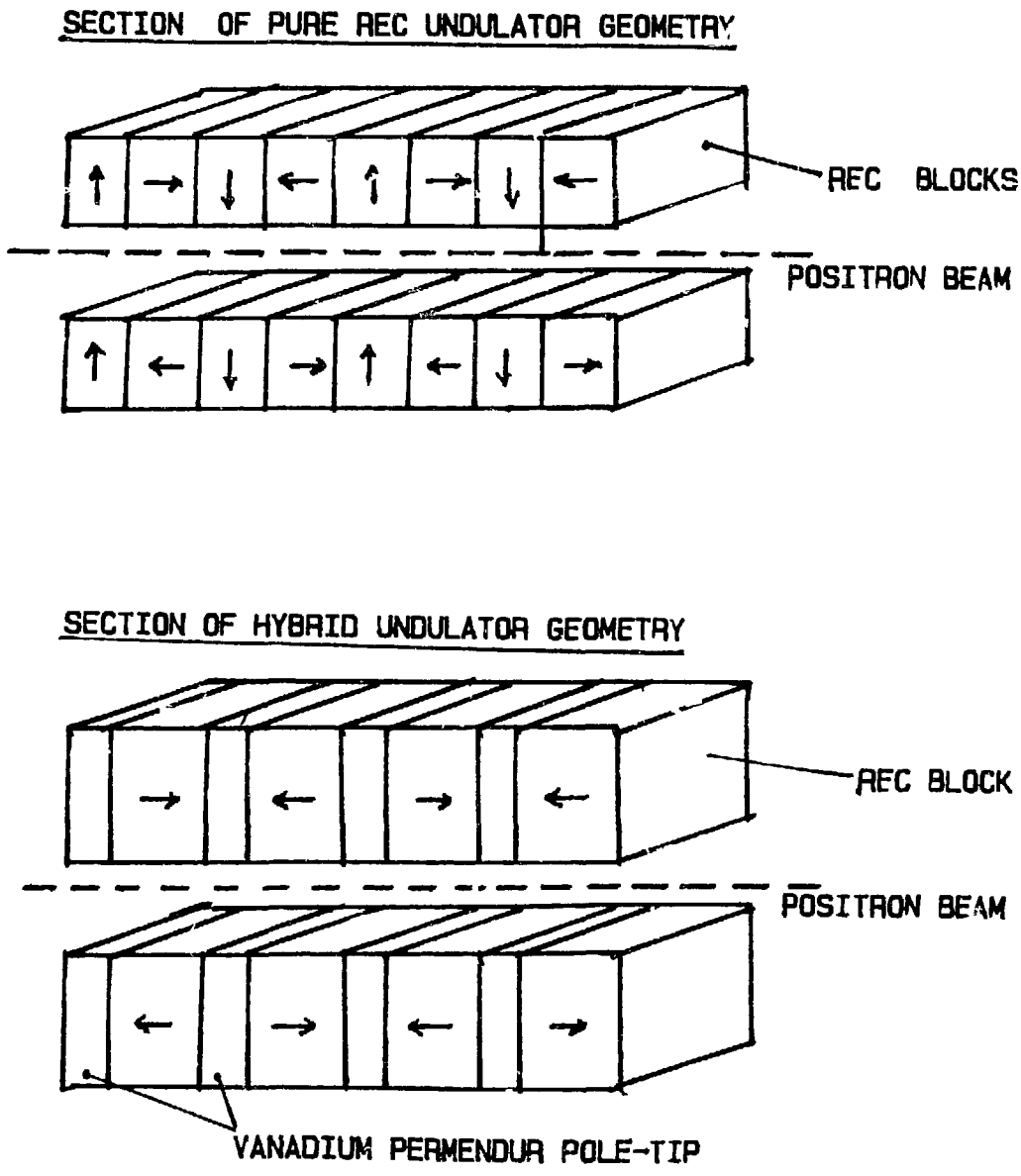

Fig. 11. Section of the magnet arrangements in a pure REC and a hybrid undulator. The end-correction devices have not been shown.

peak field B_o on the magnet gap G (cm) and undulator period λ_o (cm) is given by

$$B_o\ (T) = 3.33 \times 0.95 \times \exp[-G/\lambda_o\ (5.47 - 1.8\ G/\lambda_o)] \qquad (11)$$

for $0.07 \leq G/\lambda_o \leq 0.7$. Since B_o is governed by the ratio G/λ_o (see Fig. 12), an increase in the gap will demand an increase in λ_o to keep B_o a constant. The factor 0.95 represents the 'filling factor'. We also note that a value of $G/\lambda_o = 0.5$ gives $B_o = 0.316$ T, which is nearly the value of the field used in the above discussion.

The energies of photons along the axis of a planar (or transverse) undulator peak at approximately

$$E_i(eV) = \frac{949\ E_R^2(GeV^2)\ i}{\lambda_o(cm)\ (1 + K^2/2)}\ , \qquad (12)$$

where again

$$K = 0.934\ B_o(T)\ \lambda_o(cm) \qquad (13)$$

and i is the harmonic.

From Eqs. (12) and (13), we observe that one can, in principle, obtain any photon peak energy from an undulator by the selection of G and λ_o. However, there are two major restrictions:

1. The gap cannot be reduced below a certain minimum value, since there will be a definite aperture size needed for the positron beam. This minimum will also be governed by the details of the length of the straight section, the vacuum requirements and the procedures to meet them, etc. If the undulator is inserted in the ring vacuum, then the minimum gap can be about 0.8 cm. On the other hand, if the poles of the undulator are located outside the vacuum jacket of the straight section, the minimum gap will have to be about 1.0 to 1.2 cm to include the vacuum chamber wall thickness. If the magnet technology is improved, λ_o can be reduced to 1.0 cm or much less. The limit on λ_o is set by the requirement that $G/\lambda_o < 1$ for Eq. (11) to be applicable in the case of hybrid magnets.

2. The second constraint concerns the largest desirable value of K. As discussed in the next section, for $K > 4$ the positron deflection becomes appreciable and higher order harmonics become prevalent in the spectrum. The utility of higher harmonics ($i > 3$) is often limited in undulator applications and they add to the heat load on the optics. The value of K cannot be infinitesimally small either. Any value of K smaller than 0.2 drastically reduces the flux from the device (see next section).

For the 6-GeV storage ring, we have calculated E(i=1) vs G/λ_o for various values of λ_o. This is shown in Fig. 13. The variation of K vs G/λ_o for various values of λ_o is shown in Fig. 14. The boundaries of these figures are determined by the above-mentioned constraints, viz. G(= 0.8 cm), G/λ_o (< 1.0), K_{max} (relaxed to 3) and K_{min} (= 0.2). These diagrams can be used to define

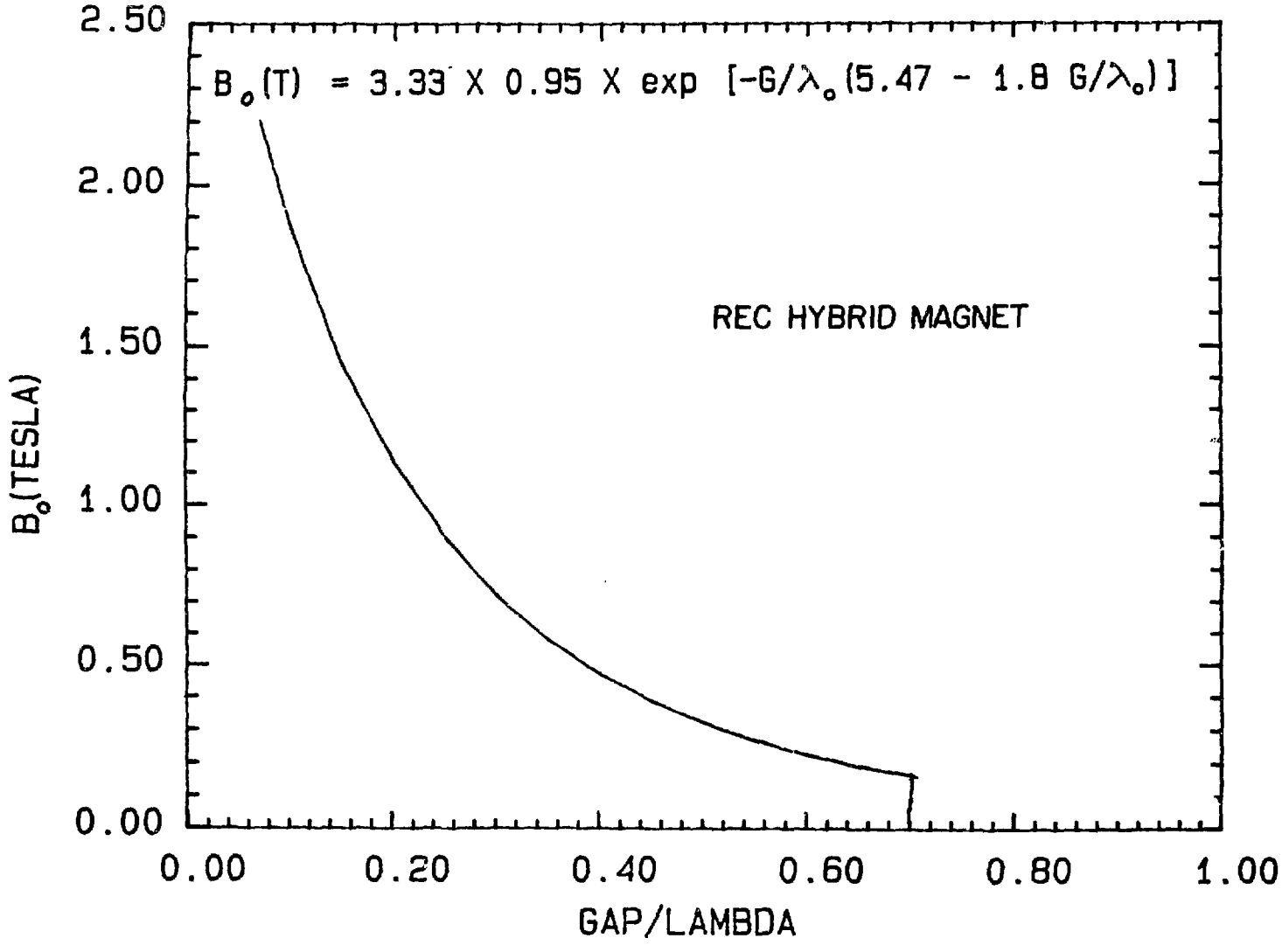

Fig. 12. Distribution of field in a hybrid magnet undulator as a function of the ratio of magnet gap and period.

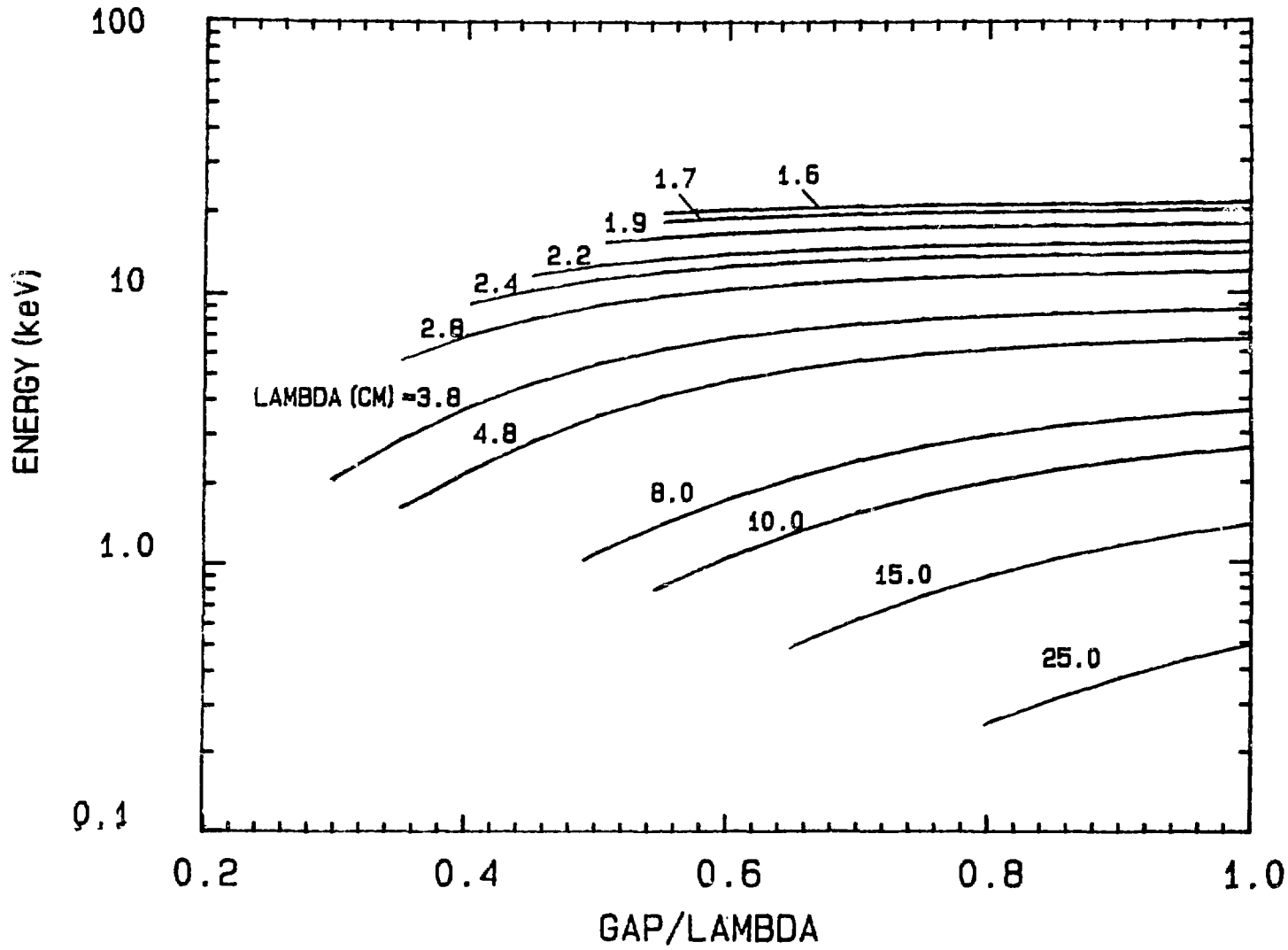

Fig. 13. Energy of radiation from a set of hybrid undulators with different periods on a 6-GeV storage ring as a function of the ratio of the magnet gap and period.

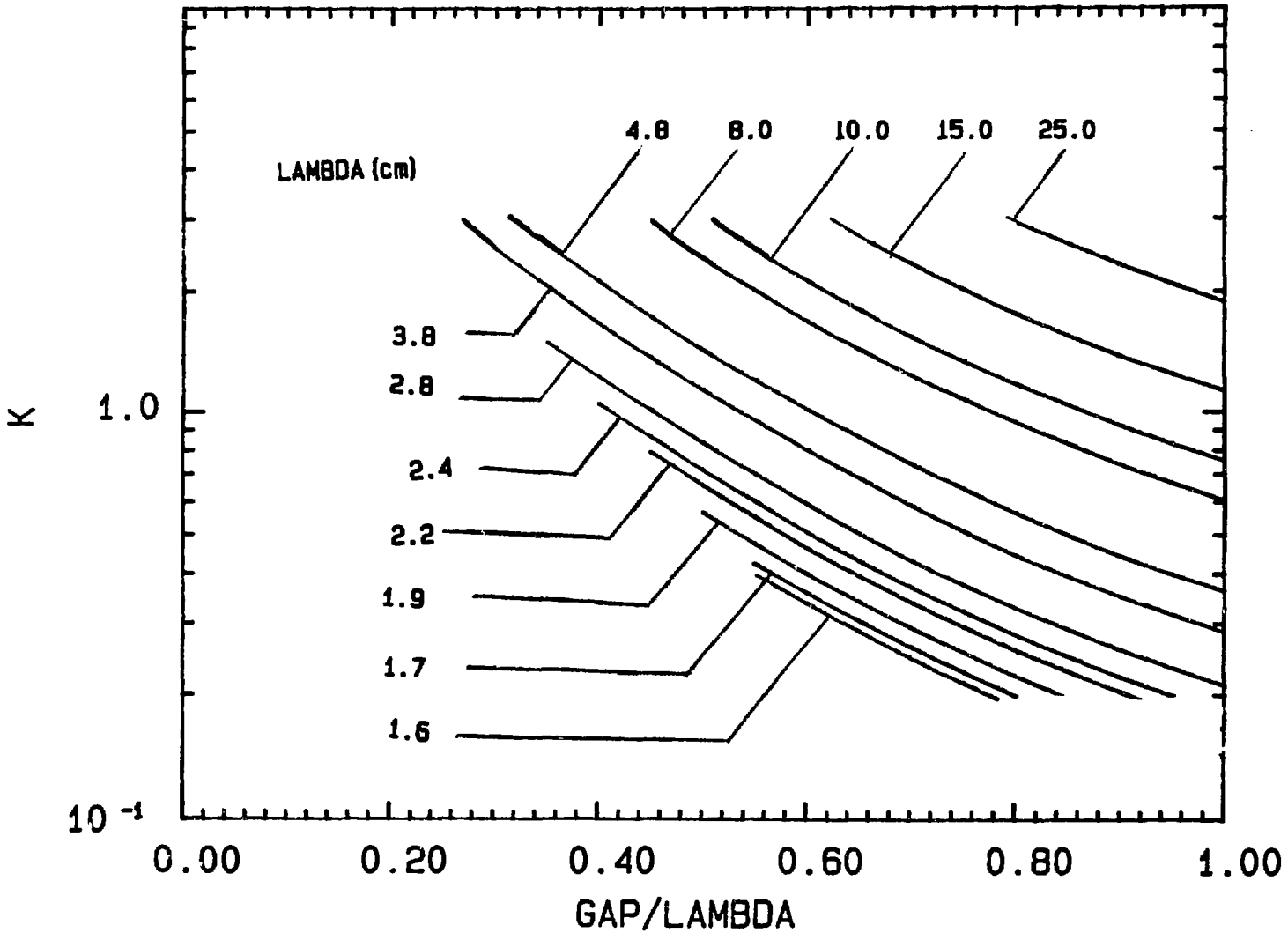

Fig. 14. Variation of the deflection parameters for a set of hybrid undulators with different periods on a 6-GeV storage ring as a function of the ratio of the magnet gap and period.

the 6-GeV hybrid undulator parameters required to deliver various first and third harmonic energies.

We wish to remind the reader that the above example of a hybrid magnet was discussed in some detail only to emphasize the simplicity of defining the undulator parameters for any specific application.

Many other aspects of the undulator design also need to be addressed by the accelerator physicist. These include the influence of undulator aperture on the ring vacuum and hence on the positron beam lifetime, the changes in the transverse and longitudinal resistivities of the RF system in the presence of the undulators and hence in the instabilities, the monitoring of the positron or photon beams in reference to the undulator axis, beam diagnostics in the straight sections, etc.

The newer magnet materials and designs mentioned above will overcome some of the minimum gap restrictions and also increase the tunable range of these devices.

C. Undulator Brilliance [3]

The average undulator brilliance can be calculated to various degrees of precision. This is discussed below in three parts. In the first, we assume that there is no angular spread in the positron beam.

1. In a "far-field approximation" (i.e., with the observer far away from the undulator), the total photon flux (angle integrated) along the undulator axis in the i-th harmonic for a planar (or transverse) undulator is given by

$$F_i = 1.43\times10^{11}\ N\ I(mA)\ U_i(K) \left(\frac{\sin N\pi i}{2N\cos\frac{\pi i}{2}}\right)^2 \quad ph/sec/0.1\%BW, \qquad (14)$$

where the undulator function is given by

$$U_i(K) = \frac{iK}{1 + K^2/2}\left[J_{\frac{i+1}{2}}(\zeta) - J_{\frac{i-1}{2}}(\zeta)\right] \qquad (15)$$

and

$$\zeta = \frac{iK^2/4}{1 + K^2/4}\ .$$

For an undulator with a large number of periods N,

$$F_i \simeq 1.43\times10^{11}\ N\ I(mA)\ U_i(K). \qquad (16)$$

The above formula is very handy for quick calculations. The behavior of the undulator function $U_i(K)$ is shown in Fig. 15. We notice that for small values of $K(<1)$, the value of $U_i(K)$ for $i = 1$ dominates over $i = 3,5,\ldots$. However, for very small K (<0.2), $U_i(K)$ is small and hence the flux from the device is drastically reduced.

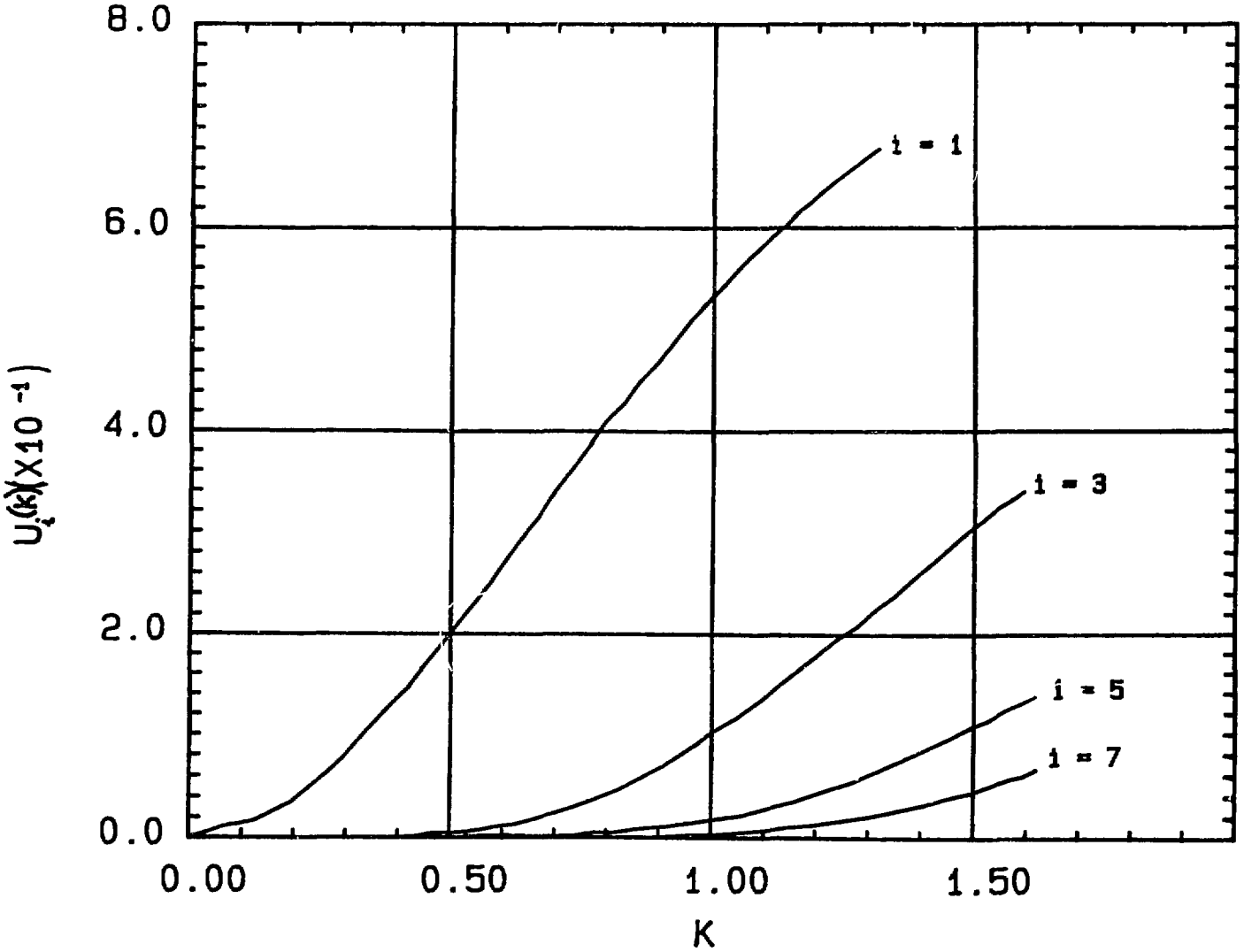

Fig. 15. Undulator function $U_i(K)$ for various harmonics i used in the calculation of undulator brilliance.

To estimate brightness along the undulator axis, the following equation may be used:

$$BT_i = 2.28\times10^{10}\ N\ I(mA)\ U_i(K)/\Sigma_x'\Sigma_y'\ \ ph/sec/0.1\%BW/mrad^2. \qquad (17)$$

The brilliance along the axis is estimated by use of the expression

$$B_i(E) = 3.62\times10^{9}\ N\ I(mA)\ U_i(K)/\Sigma_x'\Sigma_y'\Sigma_x\Sigma_y\ \ ph/sec/0.1\%BW/mrad^2/mm^2. \qquad (18)$$

The definitions of $\Sigma_{x,y}$, $\Sigma'_{x,y}$ are given in section III. In Table 5, we show the use of the above equations to indicate how they help in designing and optimizing two undulators (20 keV and 1 keV) for the 6-GeV ring.

2. It must be emphasized that to make more realistic estimates of the undulator energy spectra, the electron beam divergence and size must be included in our calculation. In addition, the energy of the photons is dependent on the observation angle θ through the equation

$$E_i(eV) = \frac{949\ E_R^2(GeV^2)i}{\lambda_o(cm)\ (1 + K^2/2 + \gamma^2\theta^2)}\ . \qquad (19)$$

The above aspects, viz. (1) beam dimensions and (2) θ dependence of photon energy, should be included in spectral calculations through Gaussian convolution of Eq. (18). Kim [3] has presented many such calculations for 6-GeV undulators. The interesting aspect of such calculations is that one observes contributions from the even harmonics (i=2,4,6...) even if the observer is along the undulator axis. In addition, these important calculations have yielded considerable insight into the dependence of brilliance on β-functions, on the number of undulator periods, etc.

3. The above formalism involves some intrinsic approximations in arriving at the analytical expressions for the flux and in convoluting the source size. A more accurate procedure is based on numerical methods in which the Lienard-Wiechert potential is integrated over the positron trajectory of finite dimensions [4]. All the spectra for the average spectral brilliance presented as examples in this report are computed by use of this formalism. These calculations demand considerable computational time, depending on various parameters such as the number of periods in the device, the integration accuracy, the ring energy, and the source dimensions.

Figures 16a through 16k present spectra for 11 different 5-m-long undulators suitable for a 6-GeV storage ring. The accuracy of integration is reduced for short-period undulators to save on computational cost. In each of these figures (except Figs. 16j and 16k), we present two spectra which correspond to two values of the gap for a single undulator. The energy spanned by these undulators varies from about 20 keV to 250 eV in the first harmonic. One can clearly see the second and the third harmonics.

It is worthwhile to make a few remarks regarding the width of the undulator peaks. For a single positron passing through an undulator, the width of the odd harmonics observed at a fixed angle θ is given by

Table 5. Examples of Flux Brilliance Estimates for Simple Hybrid Transverse Undulators
(β_x = 29.5 m, β_y = 7.3 m, L = 5 m, I = 100 mA)

λ_o (cm)	K	i	E (keV)	Σ_x (mm)	Σ_y (mm)	$\Sigma_{x'}$ (mrad)	$\Sigma_{y'}$ (mrad)	Flux (ph/sec/0.1%BW/mrad θ)	Brilliance (ph/sec/0.1%BW/mrad^2/mm^2)
1.54	0.46	1	20.0	0.43	0.068	0.015	0.010	8.4×10^{14}	4.7×10^{18}
		3	60.0	0.43	0.068	0.015	0.009	1.3×10^{14}	7.6×10^{16}
		5	100.0	0.43	0.068	0.015	0.009	2.0×10^{11}	1.3×10^{15}
13.1	1.79	1	1.0	0.43	0.072	0.02	0.018	4.5×10^{14}	9.3×10^{17}
		3	3.0	0.43	0.069	0.017	0.013	2.0×10^{14}	7.5×10^{17}
		5	5.0	0.43	0.069	0.016	0.012	1.0×10^{14}	4.7×10^{17}

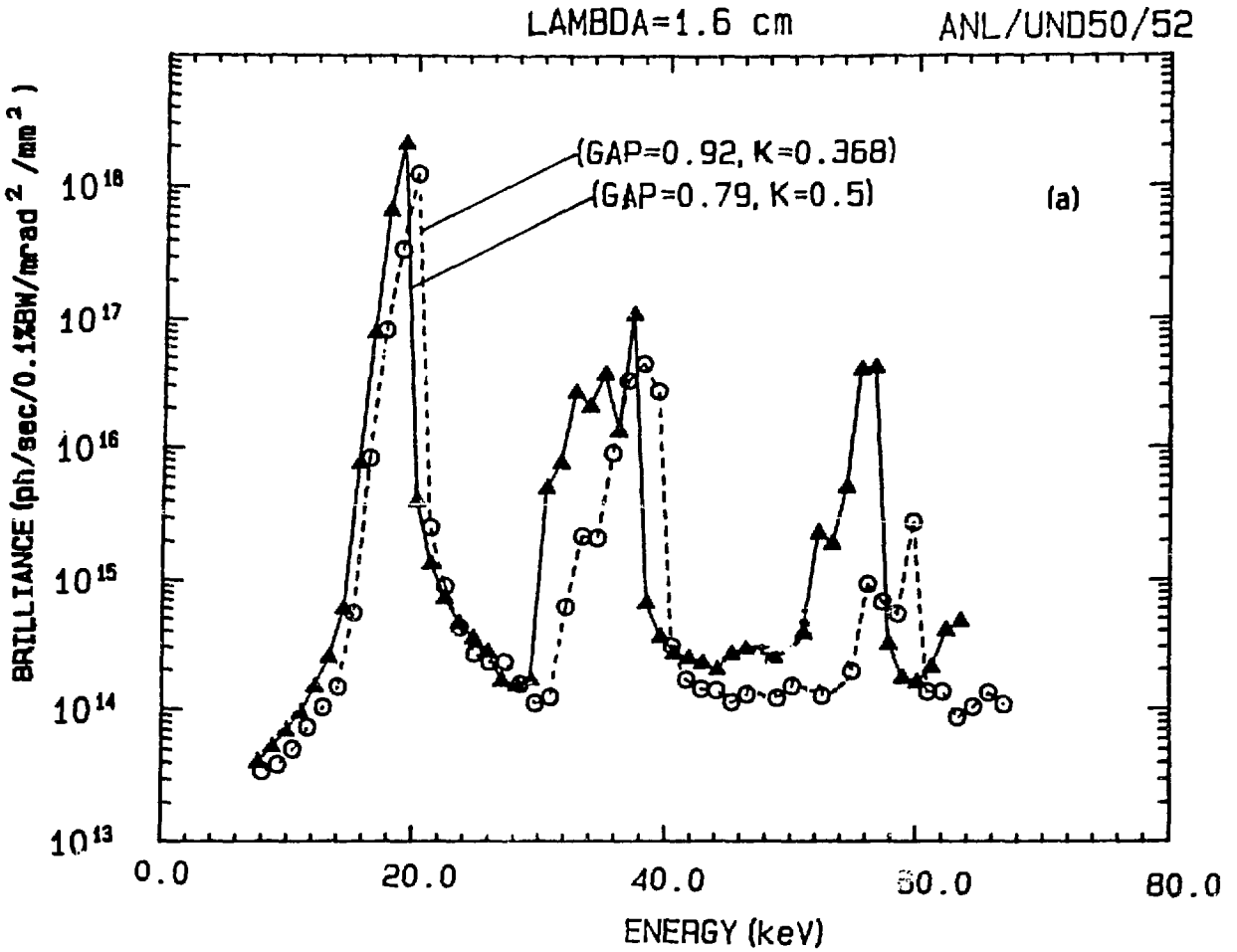

Fig. 16. On-axis brilliance vs energy for a set of 6-GeV hybrid undulators (100 mA). Calculations include the source size. Each figure corresponds to a different undulator period ranging from 1.6 to 25 cm. Most figures carry two spectra calculated for different undulator gaps. The gap values (in cm) and K are given on the curves. We have assumed each of the undulators to be 5 m long, with stored current of 100 mA.

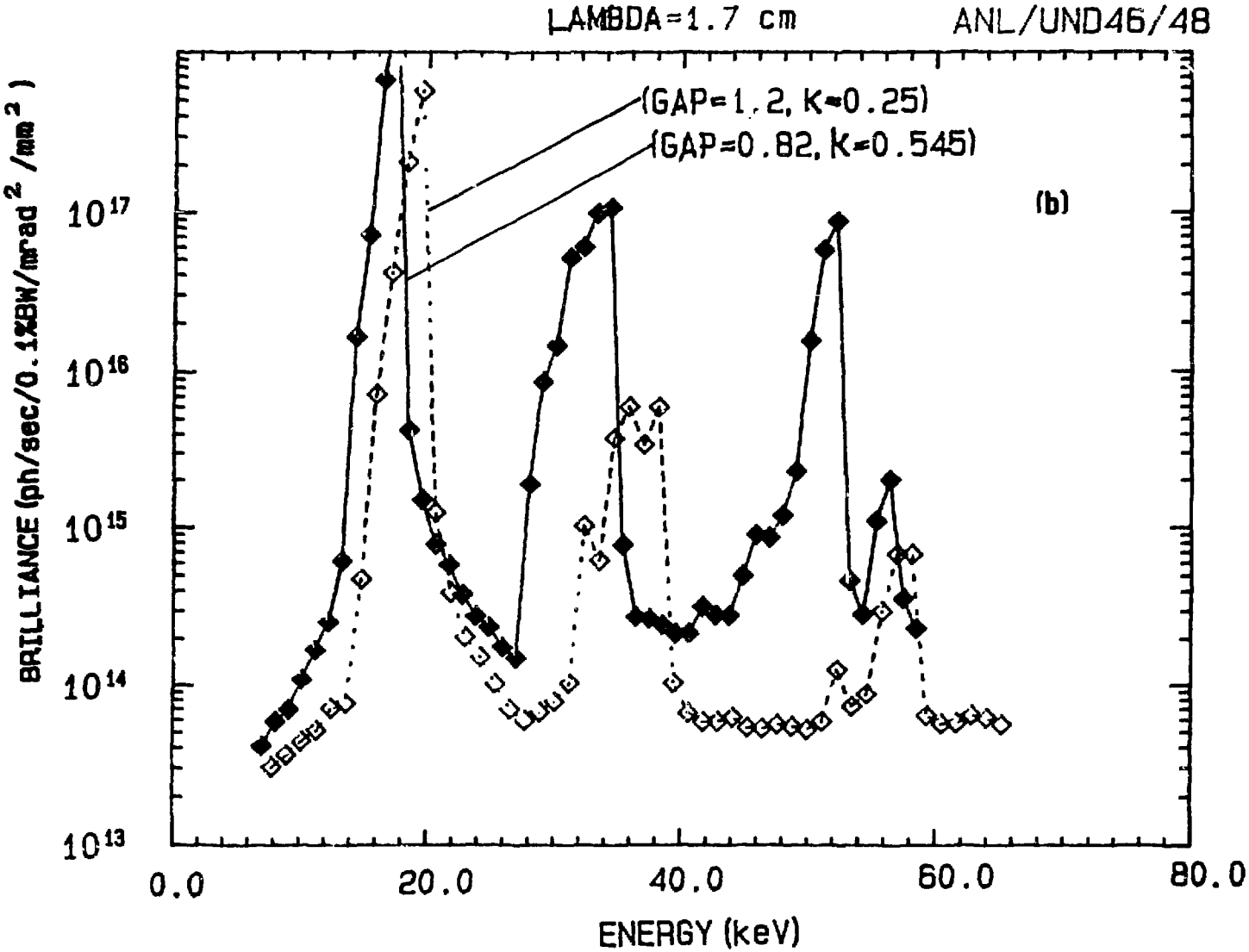
LAMBDA=1.7 cm
ANL/UND46/48
(GAP=1.2, K=0.25)
(GAP=0.82, K=0.545)
(b)
BRILLIANCE (ph/sec/0.1%BW/mrad^2/mm^2)
10^{17}
10^{16}
10^{15}
10^{14}
10^{13}
0.0
20.0
40.0
60.0
80.0
ENERGY (keV)

Fig. 16. (Contd.)

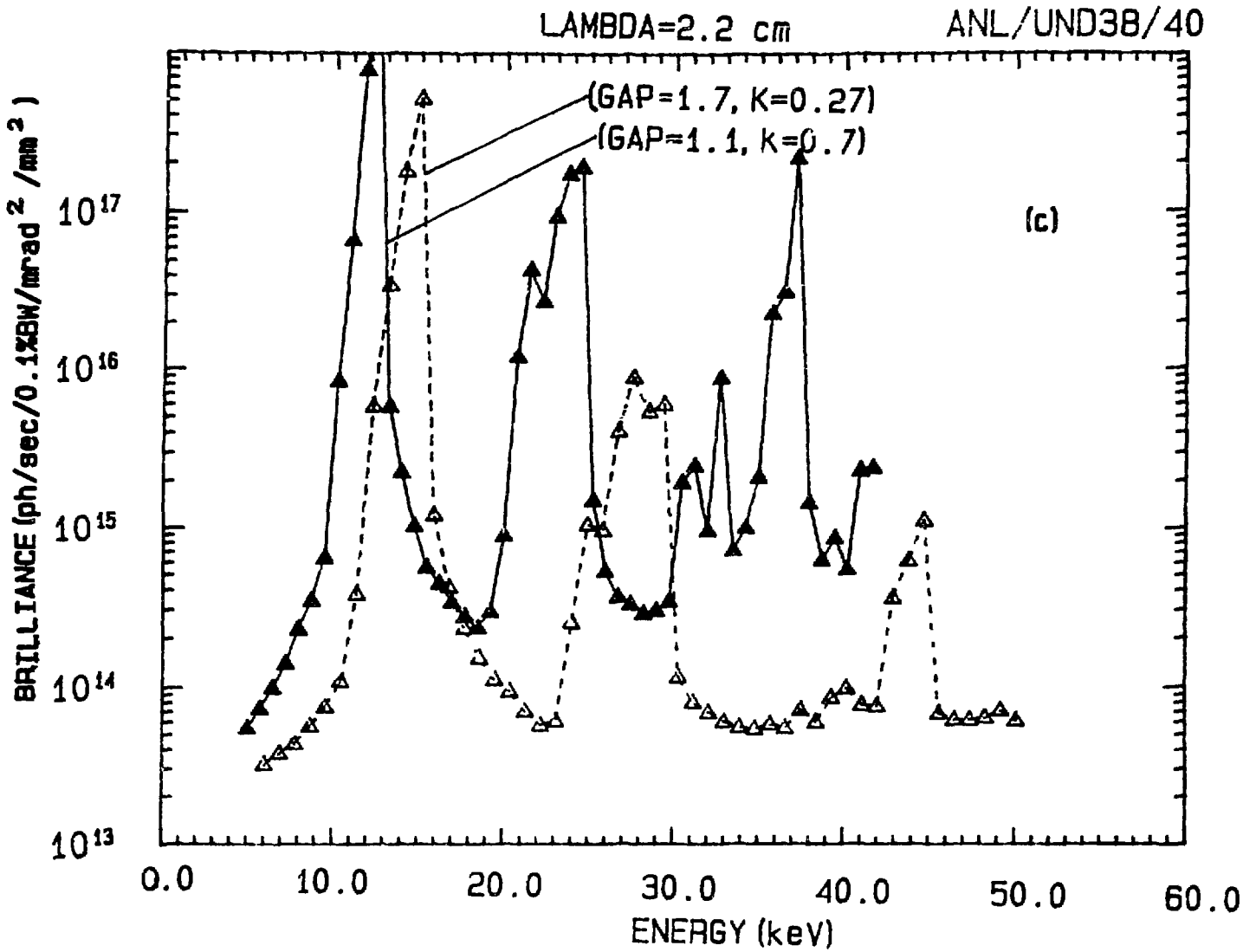
LAMBDA=2.2 cm
ANL/UND38/40
(GAP=1.7, K=0.27)
(GAP=1.1, K=0.7)
(c)
BRILLIANCE (ph/sec/0.1%BW/mrad^2/mm^2)
10^{17}
10^{16}
10^{15}
10^{14}
10^{13}
0.0
10.0
20.0
30.0
40.0
50.0
60.0
ENERGY (keV)

Fig. 16. (Contd.)

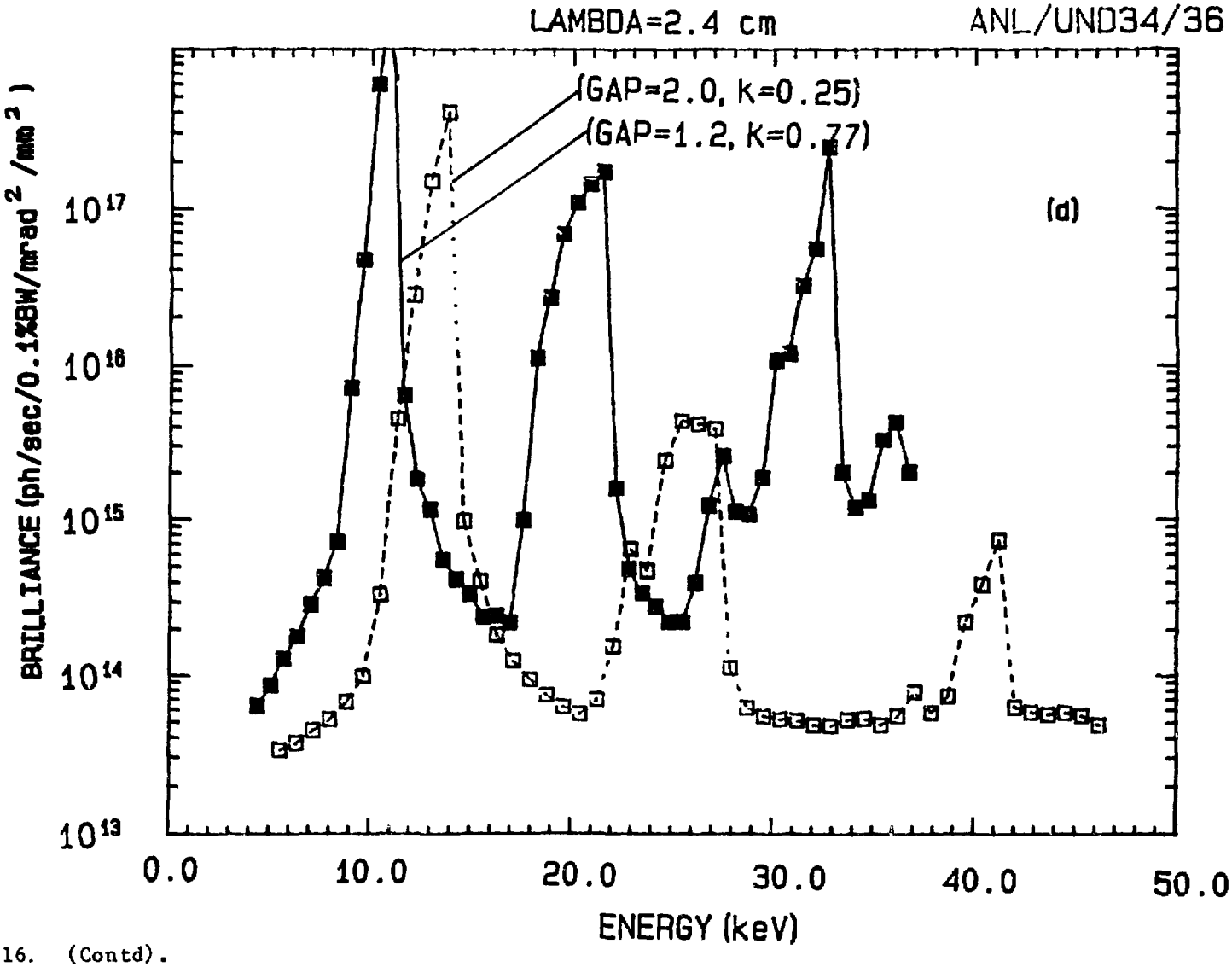
LAMBDA=2.4 cm
ANL/UND34/36
(GAP=2.0, K=0.25)
(GAP=1.2, K=0.77)
(d)
BRILLIANCE (ph/sec/0.1%BW/mrad^2/mm^2)
10^{17}
10^{16}
10^{15}
10^{14}
10^{13}
0.0
10.0
20.0
30.0
40.0
50.0
ENERGY (keV)

Fig. 16. (Contd).

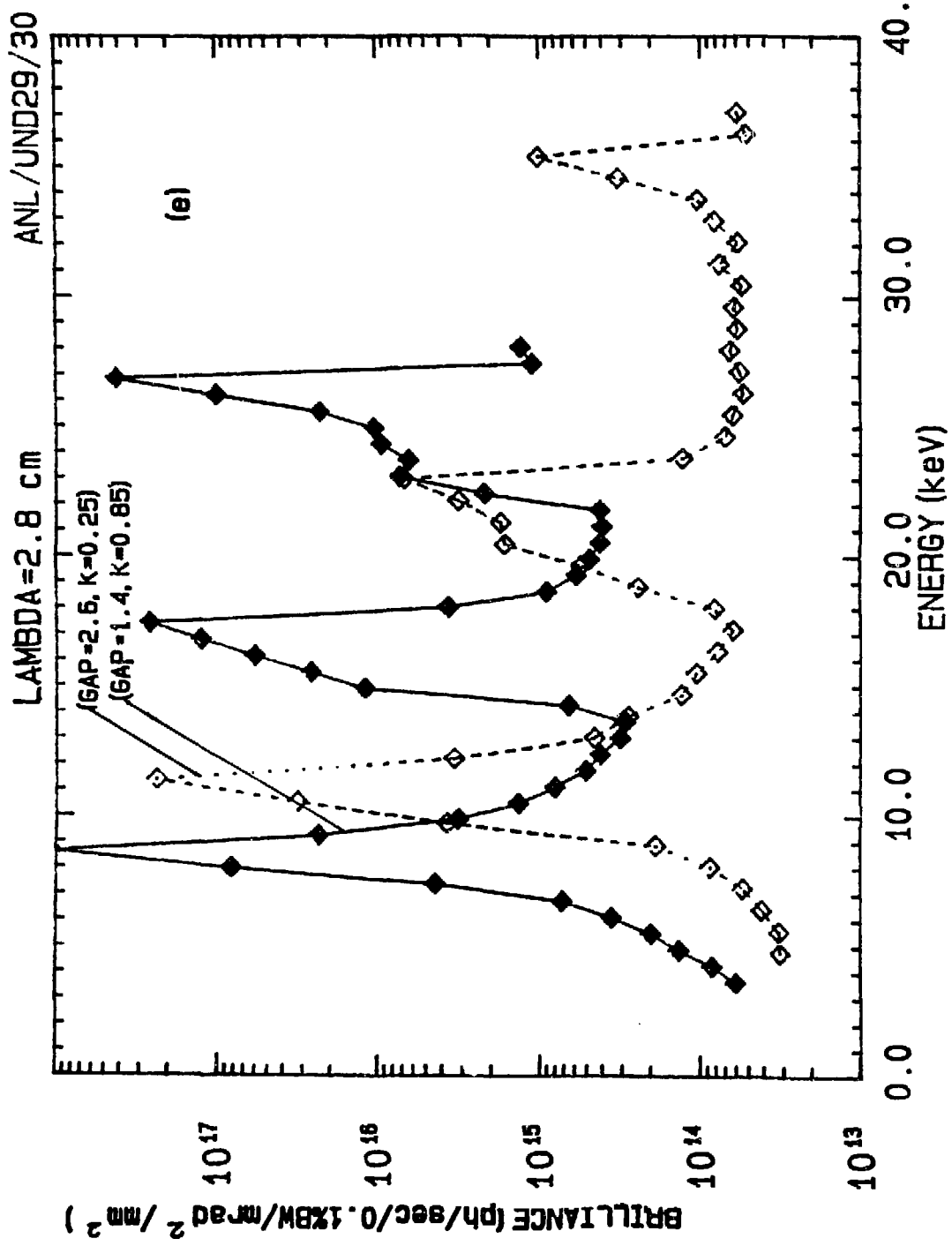
ANL/UND29/30
LAMBDA=2.8 cm
(e)
(GAP=2.6, K=0.25)
(GAP=1.4, K=0.85)
BRILLIANCE (ph/sec/0.1%BW/mrad^2/mm^2)
10^{17}
10^{16}
10^{15}
10^{14}
10^{13}
0.0
10.0
20.0
30.0
40.
ENERGY (keV)

Fig. 16. (Contd.)

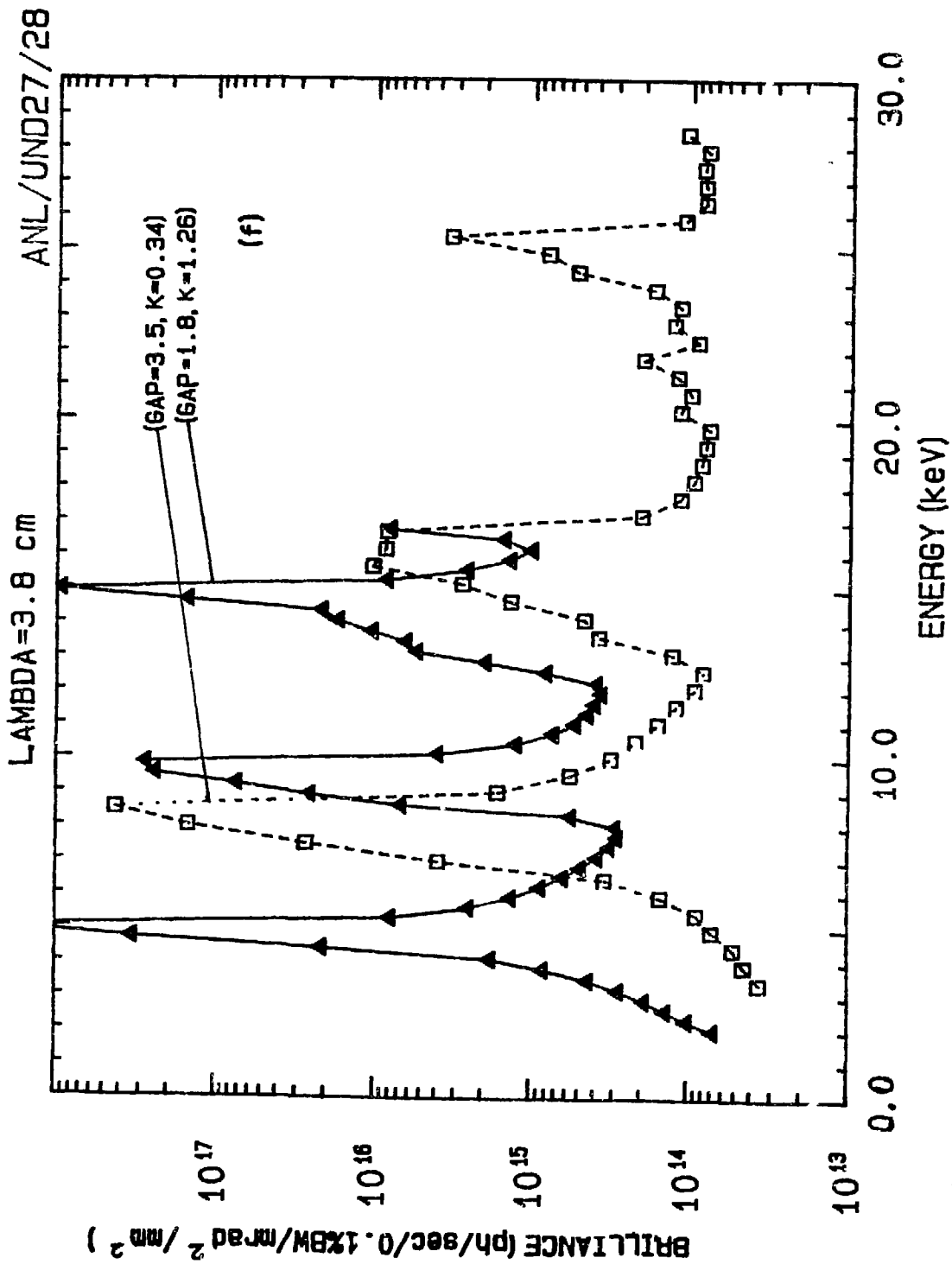
ANL/UND27/28
LAMBDA=3.8 cm
(GAP=3.5, K=0.34)
(GAP=1.8, K=1.26)
(f)
BRILLIANCE (ph/sec/0.1%BW/mrad^2/mm^2)
10^{17}
10^{16}
10^{15}
10^{14}
10^{13}
0.0
10.0
20.0
30.0
ENERGY (keV)

Fig. 16. (Contd.)

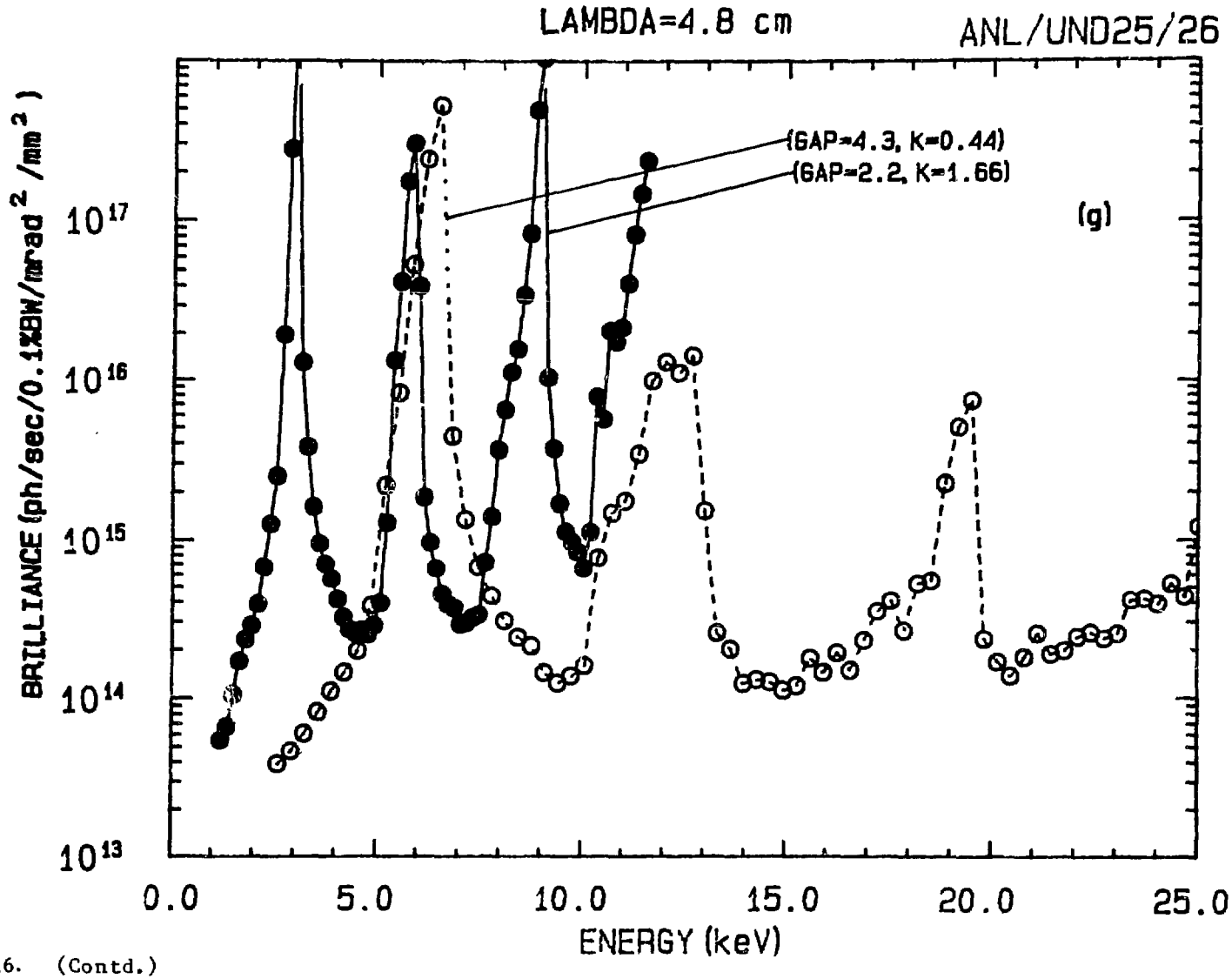
LAMBDA=4.8 cm
ANL/UND25/26
(GAP=4.3, K=0.44)
(GAP=2.2, K=1.66)
(g)
BRILLIANCE (ph/sec/0.1%BW/mrad^2/mm^2)
10^{17}
10^{16}
10^{15}
10^{14}
10^{13}
0.0
5.0
10.0
15.0
20.0
25.0
ENERGY (keV)

Fig. 16. (Contd.)

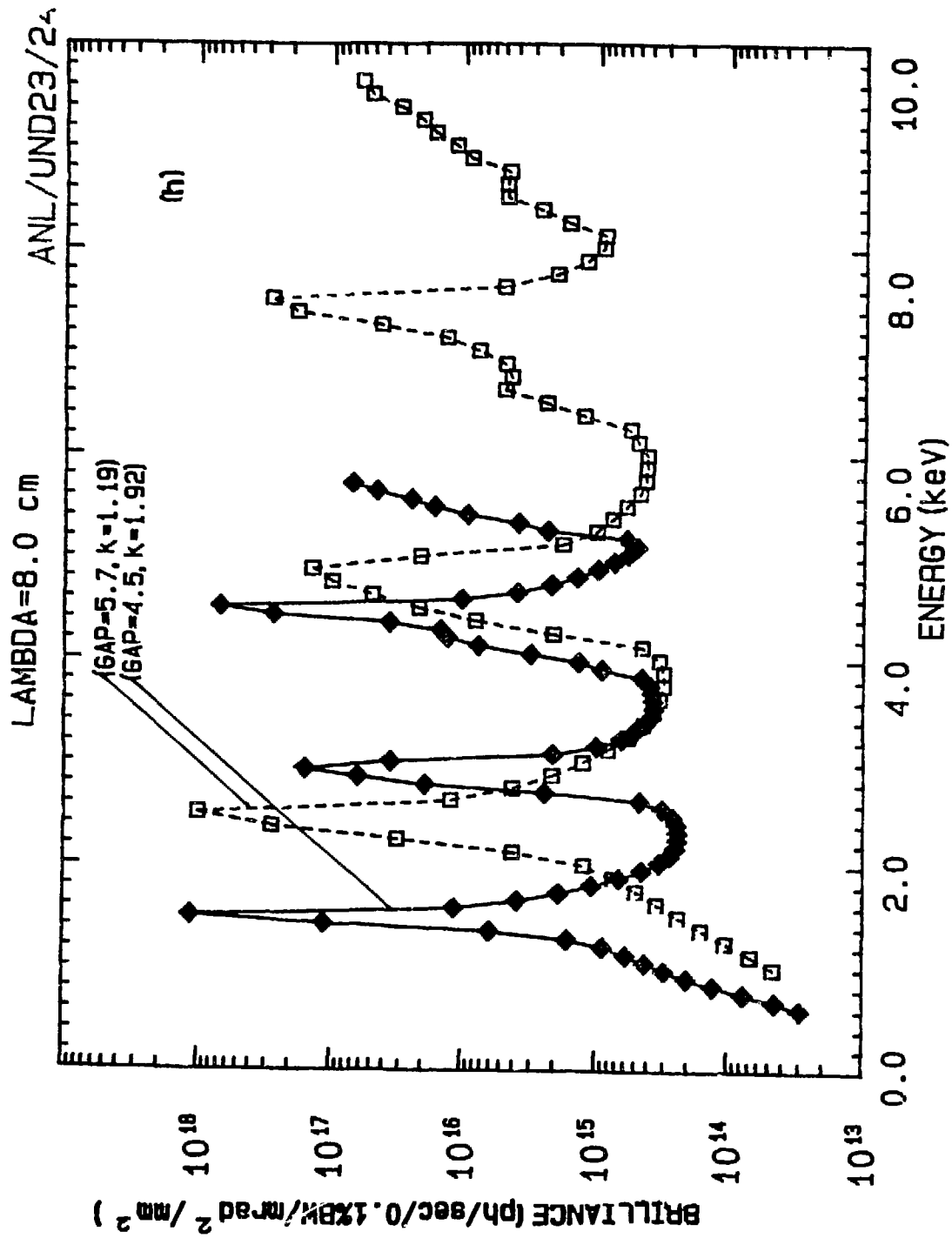
ANL/UND23/24
LAMBDA=8.0 cm
(h)
GAP=5.7, k=1.19)
GAP=4.5, k=1.92)
BRILLIANCE (ph/sec/0.1%BW/mrad^2/mm^2)
10^{18}
10^{17}
10^{16}
10^{15}
10^{14}
10^{13}
0.0
2.0
4.0
6.0
8.0
10.0
ENERGY (keV)

Fig. 16. (Contd.)

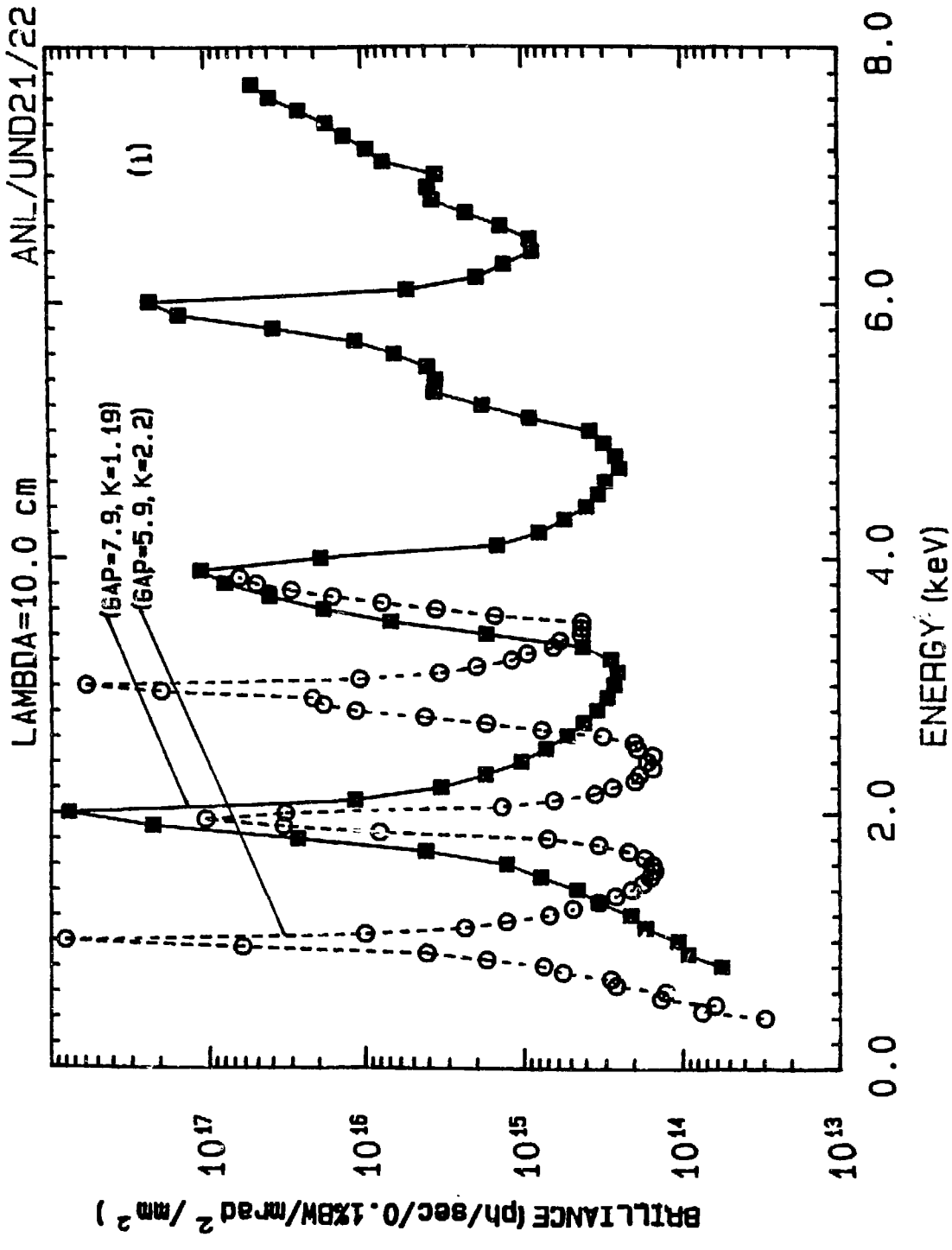
ANL/UND21/22
LAMBDA=10.0 cm
(1)
(GAP=7.9, K=1.19)
(GAP=5.9, K=2.2)
BRILLIANCE (ph/sec/0.1%BW/mrad^2/mm^2)
10^{17}
10^{16}
10^{15}
10^{14}
10^{13}
0.0
2.0
4.0
6.0
8.0
ENERGY (keV)

Fig. 16. (Contd.)

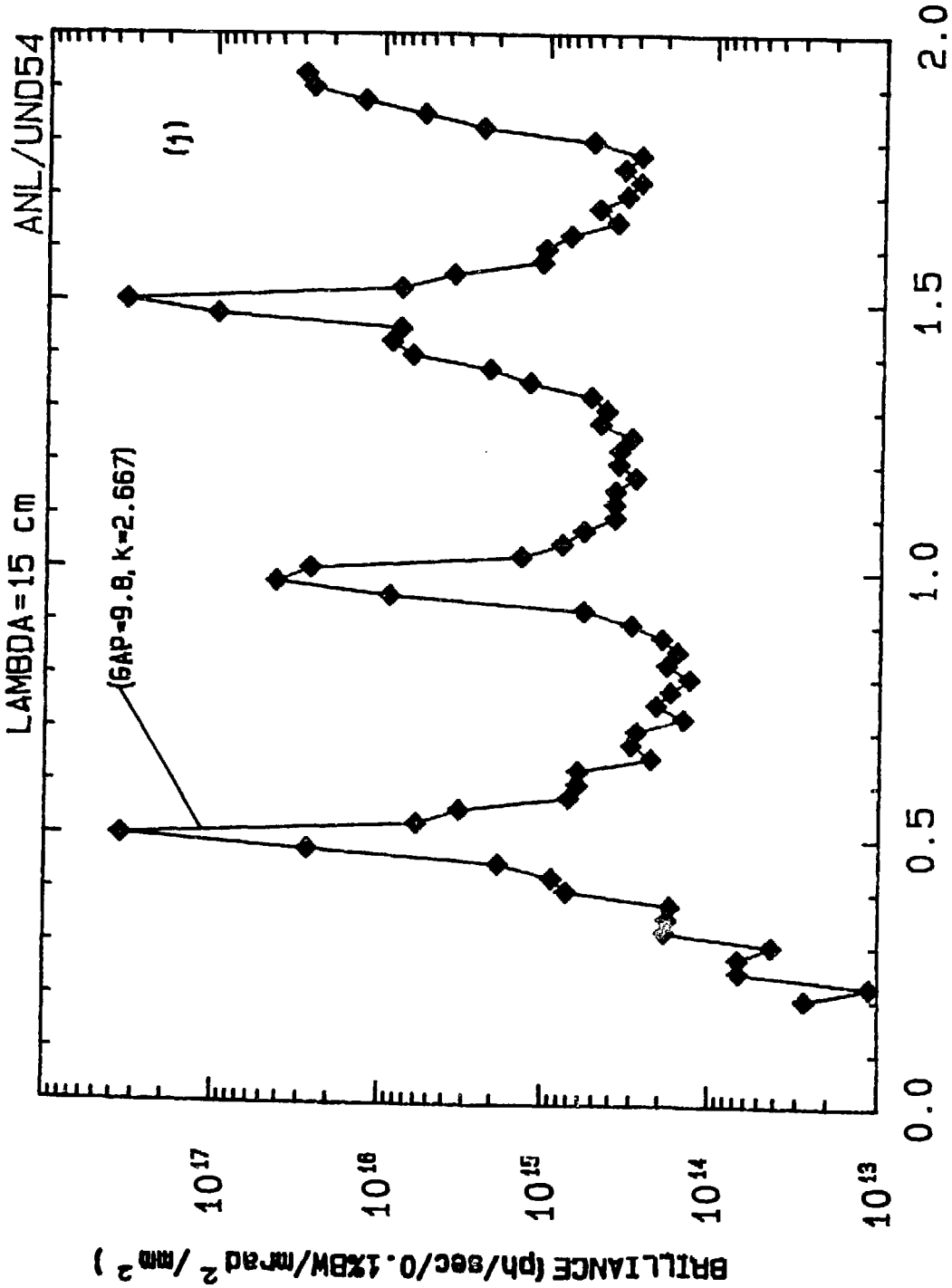
ANL/UND54
LAMBDA=15 cm
(1)
(GAP=9.8, k=2.667)
BRILLIANCE (ph/sec/0.1%BW/mrad^2/mm^2)
10^{17}
10^{16}
10^{15}
10^{14}
10^{13}
0.0
0.5
1.0
1.5
2.0
ENERGY (keV)

Fig. 16. (Contd.)

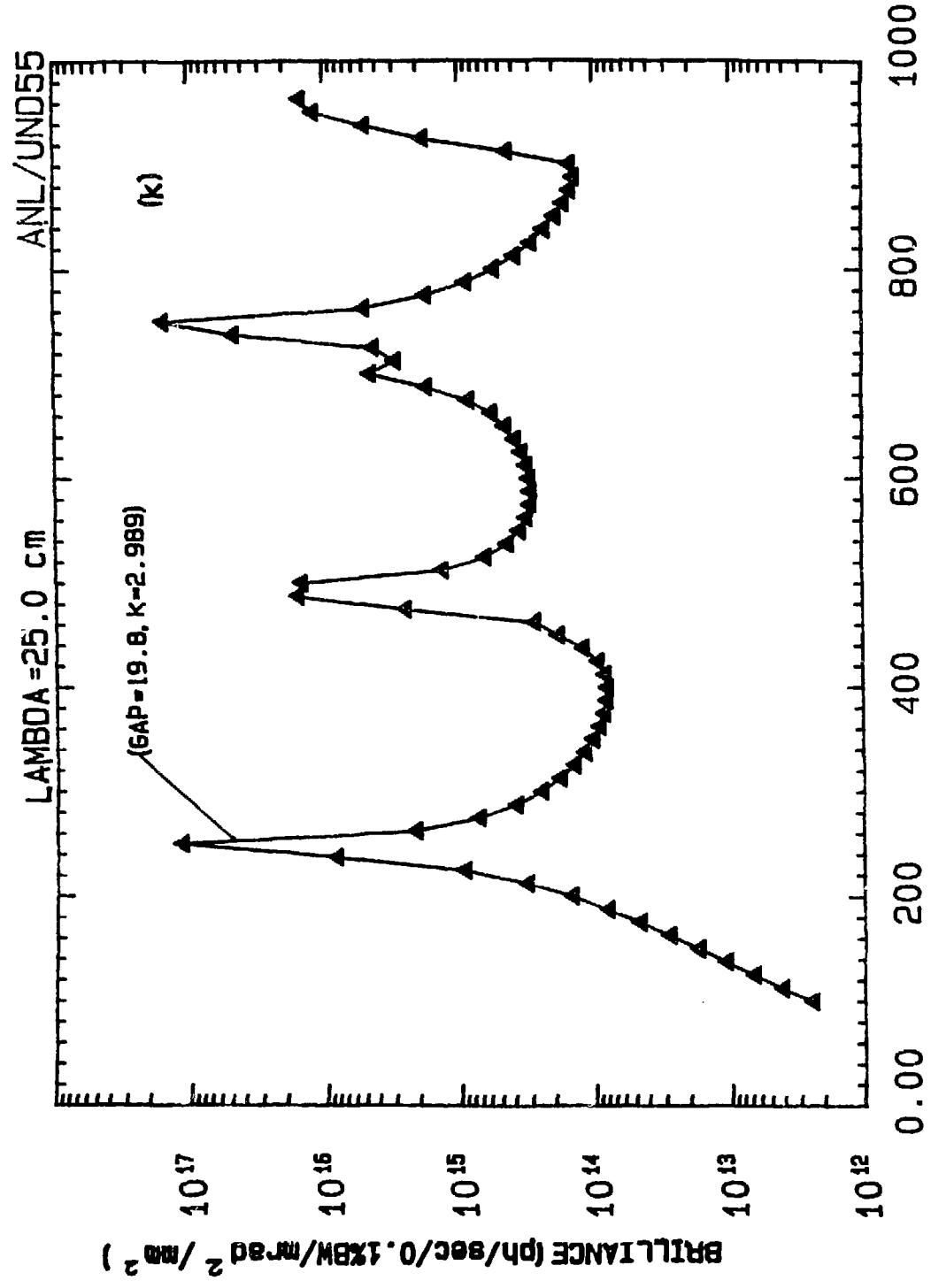
ANL/UND55
LAMBDA =25.0 cm
(k)
(GAP=19.8, K=2.989)
BRILLIANCE (ph/sec/0.1%BW/mrad^2/mm^2)
10^{17}
10^{16}
10^{15}
10^{14}
10^{13}
10^{12}
0.00
200
400
600
800
1000
ENERGY (eV)

Fig. 16. (Contd.)

$$\frac{\Delta E_i}{E_i} \approx \frac{1}{iN} \quad . \tag{20}$$

Since the energy is dependent on the observation angle θ (Eq. (19)), the angular broadening of the peak due to acceptance of radiation in a cone of half-angle $\Delta\theta$ about the undulator axis is given by

$$\frac{\Delta E_i}{E_i} = \frac{\gamma^2(\Delta\theta)^2}{1 + K^2/2} \quad . \tag{21}$$

The peak width will be as small as that given by Eq. (20) only if

$$\Delta\theta \leq \frac{1}{\gamma}\left(\frac{1 + K^2/2}{2iN}\right)^{1/2} \quad . \tag{22}$$

This has an additional consequence for a positron beam with divergence $\sigma_{x,y}'$. In order to observe the natural width of the undulator peaks (given by Eq. (20)),

$$\sigma_{x,y}' \leq \frac{1}{\gamma}\left(\frac{1 + K^2/2}{2iN}\right)^{1/2} \quad . \tag{23}$$

For our lattice, $\sigma_x' = 18$ μrad and $\sigma_y' = 7$ μrad. For an undulator with $K = 0.5$ and $N = 200$ on our ring, the right-hand side of Eq. (23) is about 4.5 μrad for $i = 1$. Thus the undulator peak widths are primarily governed by the positron beam divergence in our case, and one can never attain the natural width.

We also notice in the undulator spectra that the broadening is primarily on the low-energy side of the harmonics and the high-energy side remains sharp. This is a consequence of Eq. (19), according to which the energy of the radiation decreases as the observer moves away from the undulator axis ($\theta \neq 0$).

As discussed earlier, larger K values produce sizeable brilliance in the higher harmonics which can be used very profitably in experimentally appropriate situations. Useful flux is obtained in the central spot of angular size

$$\left\{\left[\frac{1}{\gamma}\left(\frac{1 + K^2/2}{2N}\right)^{1/2}\right]^2 + \sigma_x'^2\right\}^{1/2} \quad .$$

D. Undulator Tunability

The two spectra presented in each of nine of the above-mentioned figures (Figs. 16a-16i) clearly show an approximate range of tunability for each of these devices. The range of tunability increases for these hybrid devices on increasing the undulator period. This is in agreement with our discussion in section B.

In Figs. 17 and 18 we present the tunability information for these devices in a convenient form for i = 1 and i = 3. Note that even the i = 2 region of the spectrum is usable. The tunability range of these undulators can be increased considerably by the operation of the storage ring at a higher energy (approximately 7 GeV).

There are numerous questions regarding the undulator tunability at a 6-GeV facility. The primary one concerns the freedom of the user to change the undulator gap. Even if the experimenter demands changes in photon energy within the tunable range of the undulator, such changes demanding gap variation on an "hour-to-hour" basis should be discouraged. At most, such tuning should be permitted once just prior to the next "injection," and preferably only once in 24 hours or so. The undulators will deliver a fairly wide energy distribution and most of the experiments will need a monochromator. Thus the selection of the photon energy can be accomplished by the use of monochromators rather than through varying the undulator gap. Note that even in the valley of the undulator energy spectrum, the photon brilliance is often higher than that delivered by BM sources. This operational style will require detectors with fairly wide dynamic ranges.

The tunability of an undulator varies between 5% and 50% of the fundamental and the third harmonic photon peak energies (see Figs. 17 and 18). If a larger variation of photon energy is desired at a given beam port, then the experimenter should use either the radiation in the higher harmonic range at the cost of peak brilliance, or a set of undulators with different first harmonic energies which can be assembled at a single straight section on a carousel. The undulator switching should also be done discretely.

To establish procedures and controls over "free" access to vary the gap by the experimenter, effective "locks" (software) can be installed at each of the undulators, under the control of accelerator operations. The experimenter notifies operations of a need to change the gap prior to the next injection. Operations will "unlock" the undulator so that the experimenter can proceed to vary the gap. After the gap variations have been completed, all the undulators will be "locked" and operations will proceed with the injection. This scheme assumes that the device gaps need not be opened during injection. (This assumption may prove incorrect; if the operations require a beam-stay-clear gap (>G), the undulator gaps, particularly G $\leq$ 1.5 cm, will have to be opened for injection.) This procedure, although cumbersome, is the only route to successful operation of a 6-GeV storage ring. It will make the operations of the ring smoother and there will be satisfied users.

To summarize, undulator tuning through gap variation is desirable at a 6-GeV storage ring; however, this should not be allowed on an ad lib basis. The gap-varying procedure should be structured so that it is done just prior to an injection. Users whose experiments cannot meet this restriction are better off using BM or wiggler sources.

E. Undulator Design Tolerances

The design parameters of an undulator can be selected by using the procedures and computations suggested in the previous sections. All aspects of the technical and engineering design need careful consideration. These

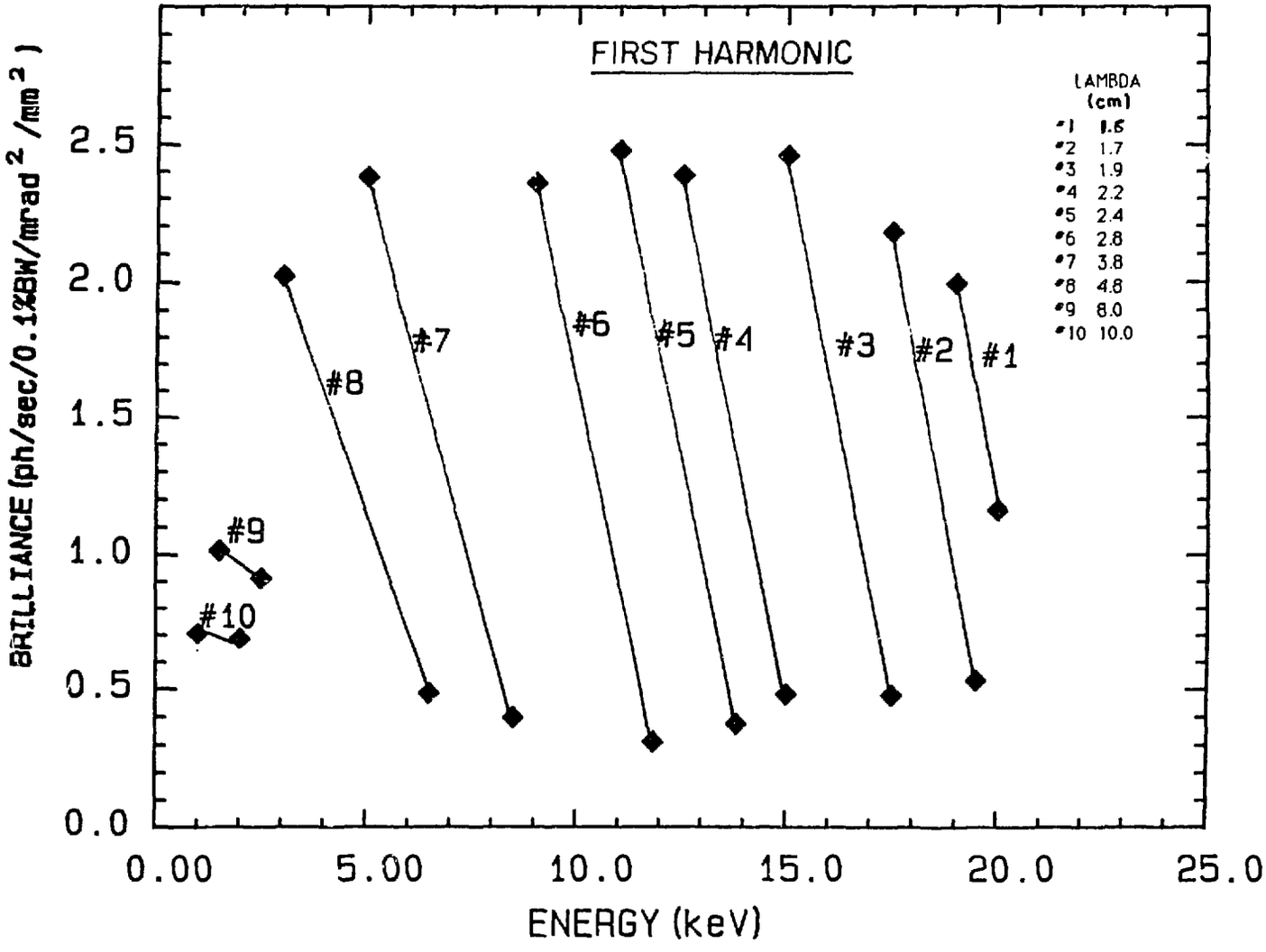

Fig. 17. Tunability range expressed as first harmonic energy vs brilliance for some typical undulators for the 6-GeV storage ring (100 mA). The undulator periods are as shown.

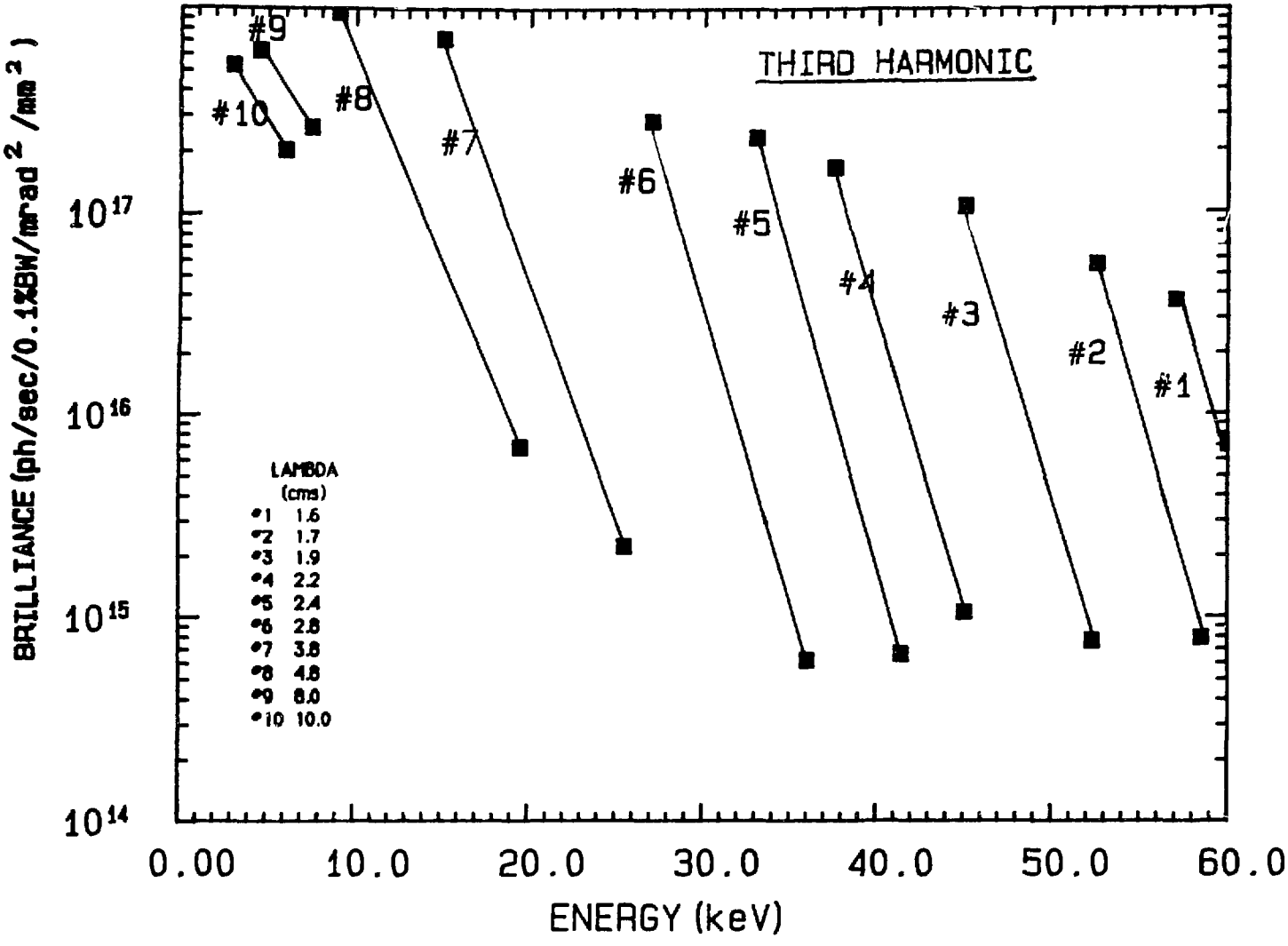

Fig. 18. Same as in Fig. 17 for the 3rd harmonic.

include a spread in λ_o along the length of an undulator, non-ideal field distribution, non-uniform gap, etc.

Inhomogeneity of the field will be detrimental to the production of high brilliance. Such variations in the field, ΔB_o, will broaden the undulator peak:

$$\frac{\Delta E}{E_1} = \frac{K^2}{1 + K^2/2} \frac{dK}{K} = \frac{K^2}{1 + K^2/2} \frac{\Delta B_o}{B_o} . \qquad (24)$$

The pole pieces have to be chosen with care to ensure well-matched magnet pairs, which will reduce ΔB_o. Careful assembly of the magnets is also crucial to the proper definition of the positron trajectory. Hence, the field distributions will have to be measured after all the pole pieces are assembled. Integral field measurements should be carried out to make sure that the field integral is zero over each half of the undulator for all field levels (various gaps). Specifically designed end poles (REC or electromagnetic) are needed for nulling the field integral. The above-mentioned effects are less important in hybrid magnets (K. Halbach, unpublished results). The field integrals can in principle be eliminated by joining shorter compensated modular lengths to build a long undulator.

Even if the pole pieces are selected with great care to reduce ΔB_o and are assembled to form a "perfect" undulator, the misalignment of the undulator axis with respect to the positron trajectory will still ruin the vertical field homogeneity. ΔB_o is a function of vertical misalignment and the undulator period. The extent of the field aberration will be greater in small-period undulators with small gaps. This necessary alignment is accomplished through remotely driven vertical, horizontal and yaw movements to make the undulator axis coincide with the 6-GeV positron orbit. It is hoped that the "golden" orbit can be realized after every injection without repeating the alignment procedure each time. In summary, the measurement of various tolerance factors at every stage of undulator assembly and installation becomes rather important. However, the tolerance requirements are likely to be less stringent for the first few harmonics in the 6-GeV case because of the inherent broadening due to beam divergence.

F. Angular Distribution and Polarization of Transverse Undulator Radiation

The angular distribution of radiation from an undulator is fairly complex, and is different for different observed harmonics of radiation [5]. We shall only present here angular distribution calculation for an undulator on a 6-GeV storage ring in which the source divergence is convoluted. In our calculation the angles θ and ϕ are defined as shown on the next page.

In Fig. 19 we show the variation of the undulator brightness as a function of θ (for $\phi = 0$) and ϕ (for $\theta = 0$). These represent the variation along the y-axis and x-axis, respectively. From this figure, we observe the peaks from higher harmonics predicted by Eq. (19).

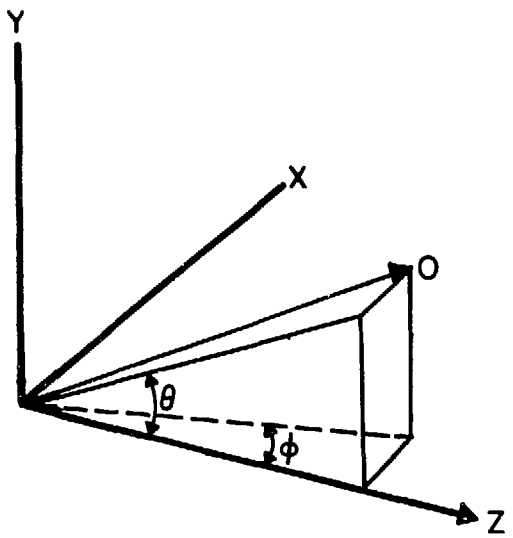

The nature of the polarization of radiation emitted by a planar undulator is dependent on θ and ϕ. The inclusion of positron beam divergence smears the polarization components from that of single-positron calculations; however, they are not destroyed. In Fig. 19 we show the σ- and π-components of polarization. The contributions to the polarization at various angles clearly originate in different harmonics. Along the x-axis one has pure σ-polarization, whereas along the y-axis the σ- and π-components appear at various angles. Our calculations suggest the possibility of selecting a wide variety of ellipticities of polarization by choosing the appropriate angle (θ,ϕ) for any undulator energy at harmonic.

G. Arbitrarily Polarized Radiation from Undulators

There are two distinct types of undulators which can in principle deliver on-axis radiation that is not only linearly polarized, unlike the planar (or transverse) undulator that we have discussed thus far. They are (1) helical undulators and (2) crossed undulators. Undulator radiation with a varying degree of polarization (linear, circular or elliptical) has the potential for numerous new applications. These include studies of biomolecules, dichroism, bulk and surface magnetic scattering, spin-polarized photoemission, and compton spin scattering, to mention just a few.

In the helical undulators, the magnets are so arranged that the positron travels in a helical trajectory. These undulators deliver circularly polarized radiation along the axis [6]. However, they have not been seriously considered for any of the storage rings because of their unacceptable influence on the storage ring. Their narrow aperture will strongly interfere with the positron beam injection. Construction of such a device demands a very close interaction between the accelerator physicists and the users. For

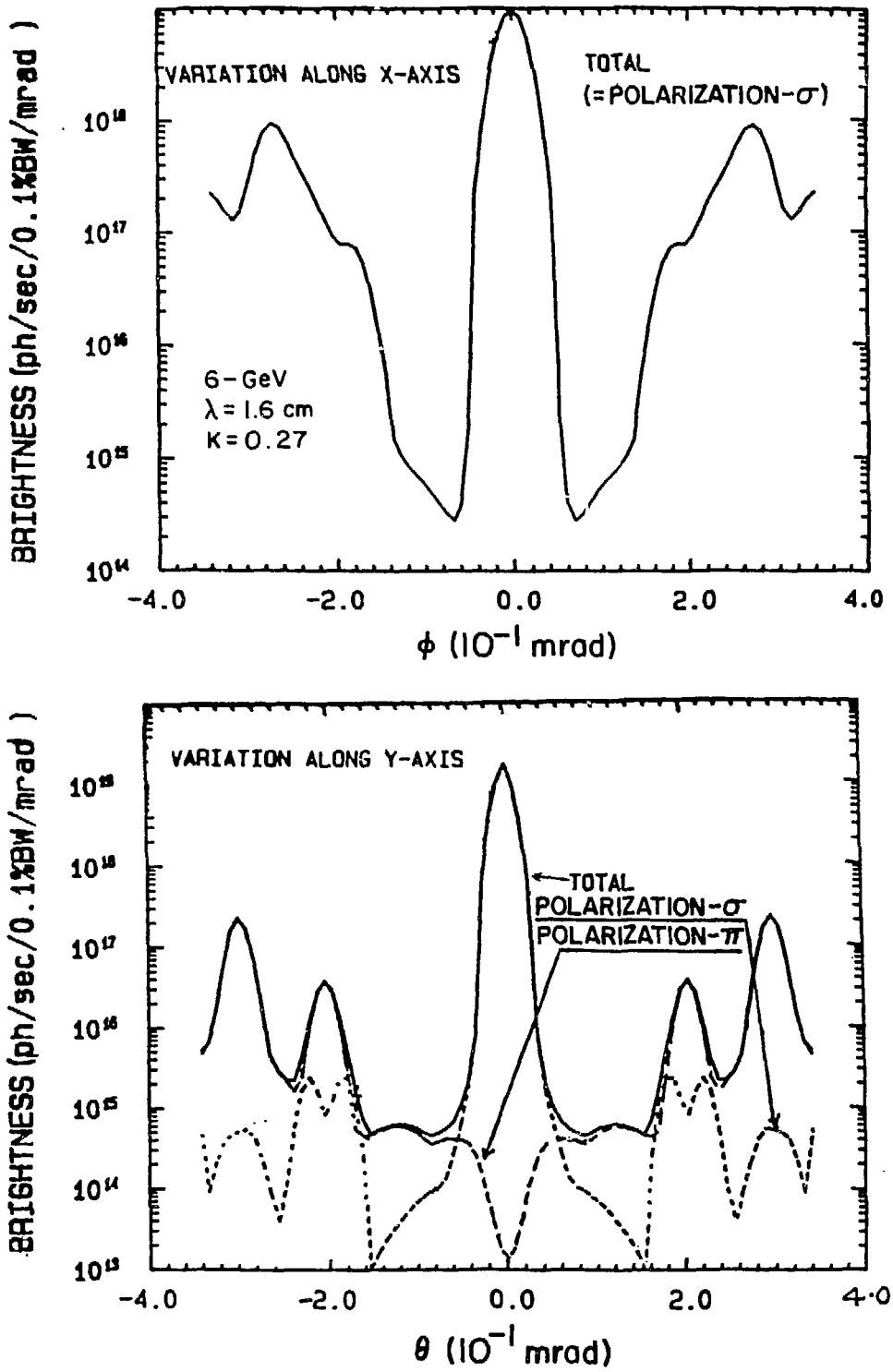

Fig. 19. Angular distributions of 20-keV radiation from a 6-GeV undulator along x- and y-axes. The σ- and π-polarization components are shown in the figure. These brightness calculations, which include the source size, assume a stored current of 1 A.

completeness, we present simple equations to estimate the first harmonic energy (at $\theta = 0$) and flux for a helical undulator:

$$E_1(\text{eV}) = 949 \frac{E^2(\text{GeV}^2)}{\lambda_o(\text{cm})(1 + K^2)} \tag{25}$$

and

$$F_1 = 2.86\text{x}10^{11}\ I(\text{mA})\ N\ K^2/(1 + K^2). \tag{26}$$

Kim [7] has proposed the so-called "crossed-undulator," which consists of a set of two orthogonal plane undulators (Fig. 20). A crossed undulator can produce polarized radiation of varying ellipticity. This is achieved by the additional magnet pair between the two undulators (Fig. 20) which introduces the necessary phase lag between the radiation from the two undulators. Such a device should be designed and tested on an existing ring before it is considered for a 6-GeV ring.

VI. WIGGLER SOURCES (K >> 1)

The critical energy of the photons and the flux can be increased by introducing a wiggler in a straight section of a ring. From the point of view of a 6-GeV storage ring, two types of wigglers need to be considered: the Energy Shifter and the Multipole Wiggler.

The first device, as the name implies, increases the critical energy of the emitted spectrum to a value higher than the BM critical energy (16 keV). For the 6-GeV storage ring, the critical energy is given by

$$E_c\ (\text{keV}) = 23.94\ B_o(\text{T}) \tag{27}$$

and $B_o = 3$ T gives $E_c = 72$ keV. Such a device usually has 3 poles, with the field of the outer two poles weaker than that of the central magnet. The outer poles act as compensating magnets to match the positron trajectory with the ring. We anticipate that such a device would be built with either Nd-Fe-B magnets or superconducting magnets, depending on the desired critical energy. One of the important applications for such a device is energy-dispersive diffraction ($E_c \sim 100$ keV). Increasing the number of poles on such a high-field device on a 6-GeV storage ring would produce radiation suitable for unusual applications.

A multipole wiggler on a 6-GeV storage ring is expected to be a low-field device (0.5-1.5 T). These fields can be obtained with current hybrid-magnet technology. The number of periods may vary from 10 to 30, depending on the application and the heat-load handling capabilities of the optics. Multiple wigglers will find many uses; we list some of the most important ones below.

- Compton scattering: charge
  ($E_c \sim 90$ keV, 20 poles).
- SEXAFS, surface diffraction, standing-wave applications
  ($E_c \sim 25$ keV, 20-30 poles).

- Conventional diffraction to study micrometer-sized single crystals ($E_c \sim 20$ keV, 20 poles).
- Conventional diffraction to study powders, liquids, amorphous systems ($E_c \sim 20$ keV, 20 poles).
- Protein crystallography ($E_c \sim 60$ keV, 10 poles).
- Time resolved topography ($E_c \sim 60$ keV, 10 poles).
- X-ray absorption spectroscopy (dispersive and time resolved) ($E_c \sim 25$ keV, 20 poles).
- Angiography/microradiography (time resolved) ($E_c \sim 35$ keV, 20 poles).
- Low-energy photon sources (for XPS or for higher harmonic rejection) ($E_c \sim 2.5$ keV, 5 poles, $B_o = 0.1$ T, $K \sim 10$).

The above list is by no means exhaustive; neither are the values of E_c nor the number of poles optimal. They are presented here merely to guide the reader towards a set of parameters suitable for his own application.

A. Wiggler Power Distribution

The radiation from a wiggler source has both ψ (xz plane) and θ (xz plane or orbital plane) distributions. The power from a wiggler at $\theta = 0$, integrated for all ψ, is calculated identically to BM radiation. For a wiggler with 2N poles (or N periods),

$$P(\theta=0) = 8.66\times10^{-3}\ E_R^{\,3}(GeV^3)B_o(T)I(mA)N. \tag{28}$$

The total radiated power for a wiggler of length L is given by

$$P(W) = 0.633\ E^2(GeV)^2 B_o^{\,2}(T^2)I(mA)L(m) \tag{29}$$

or by

$$P(W) = 7.25\times10^{-3}\ E^2(GeV^2)K^2N\ I(mA)/\lambda_o(cm), \tag{30}$$

where $K = 0.934\ B_o(T)\ \lambda_o(cm)$ as in the case of undulators.

The angular distribution of the radiation in the horizontal and vertical planes is represented by

$$P(\psi,\theta) = 0.248\ E^4(GeV^4)\ B_o(T)\ N\ I(mA)\ G(\psi,\theta)\ \ W/mrad\ \theta/mrad\ \psi \tag{31}$$

with

$$G(\psi,\theta) = F(\gamma\psi)\cos\left[\sin^{-1}(\gamma\theta/K)\right], \tag{32}$$

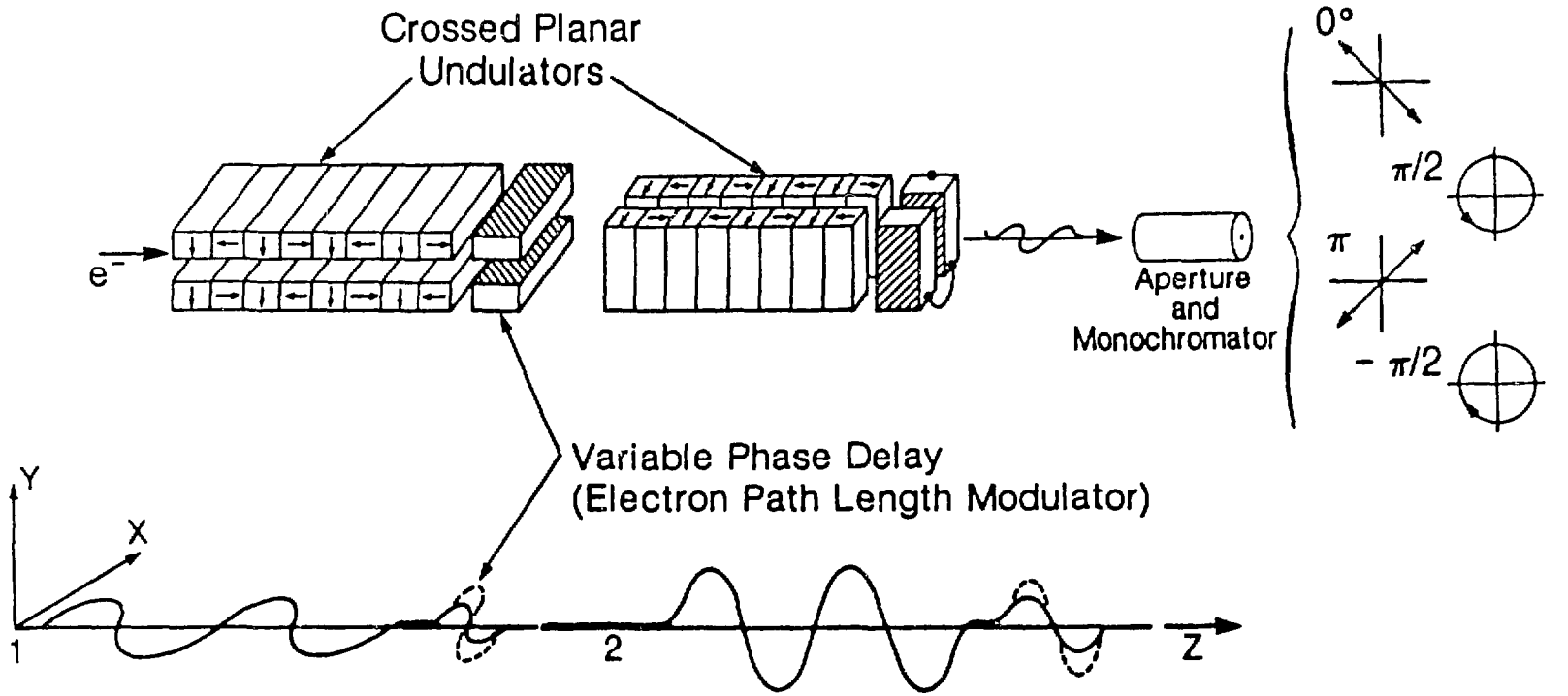

Fig. 20. A crossed-undulator scheme (presented by K.-J. Kim [7]) for producing radiation with polarization of variable ellipticity.

where $F(\gamma\psi)$ is given by Eq. (6). These detailed considerations of wiggler power distribution are essential for a careful design of the front end of the beam line. It is here that one can profit from the novel heat-load handling procedures mentioned earlier.

To illustrate, we use the following parameters for a 6-GeV wiggler: B_o = 1.5 T, N = 15, λ_o = 10 cm, K = 14, I = 100 mA. The total power from this wiggler is 7.67 kW and the peak power P (θ=0, ψ=0) is 31.6 kW. The power from this wiggler goes to zero for $\theta = \pm K/\gamma = \pm 1.2$ mrad.

In Fig. 21, the θ and ψ power distribution of the above wiggler is presented. These calculations are done for a non-divergent positron beam. The inclusion of angular spread does not greatly influence this distribution. The sharp cut-offs in power at $\theta = \pm 1.2$ mrad are smeared when beam divergence is convoluted.

It is interesting to compare wigglers on a low- and high-energy storage ring. If two wigglers, one on a 6-GeV storage ring and the other on a 3-GeV storage ring, produce photons with the same critical energy, the magnets on the 3-GeV ring should provide larger fields.

$$B_o\ (3\ \text{GeV}) = 4\ B_o\ (6\ \text{GeV}).$$

For the same current stored in both rings and for equal wiggler lengths, the ratio of the total power (Eq. (22)) will be

$$\frac{P\ (3\ \text{GeV})}{P\ (6\ \text{GeV})} = 4.$$

This is an important advantage for the high-energy ring. On the other hand, the peak power of the wiggler at $\psi = 0$, $\theta = 0$ (Eq. (32)) on the 6-GeV storage ring is 4 times that of the wiggler on the 3-GeV storage ring.

In designing optics and solving heat-flow problems, it is essential to evaluate the power densities. As we have pointed out, with high-energy storage rings, because of small θ and ψ, peak power is more pertinent for beam-line design. Following Avery [8], the peak power along the x-axis (orbital plane) can be integrated over the entire vertical plane (ψ) of radiation to obtain peak power per mrad θ (at $\theta = 0$) (Eq. (29)):

$$P_x\ (\text{W/mrad}) = 8.66\text{x}10^{-3}\ B_o(\text{T})E_R^{\ 3}(\text{GeV}^3)\text{I(mA)N}. \qquad (33)$$

The peak power per unit solid angle is

$$P_{xy}\ (\text{W/mrad}^2) = 1.076\text{x}10^{-2}\ B_o(\text{T})E_R^{\ 4}(\text{GeV}^4)\text{I(mA)N}. \qquad (34)$$

The normal radiation impinging at a distance ℓ meters from the source point (center of the wiggler length) can be defined in terms of linear and surface power densities, as follows:

Peak Linear Power Density:

$$W_x\ (\text{W/mm}) = P_x/\ell(\text{m}). \qquad (35)$$

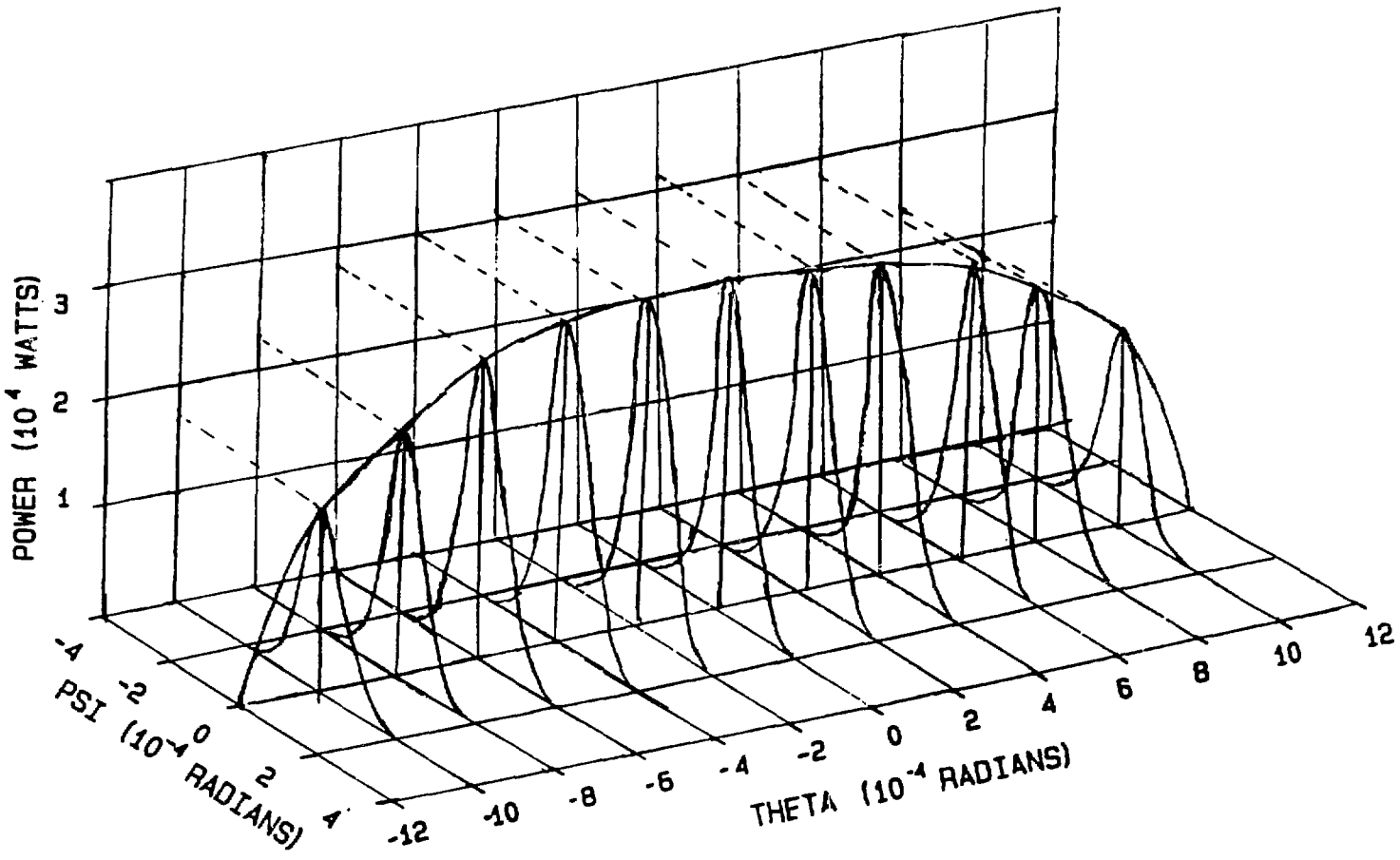

Fig. 21. Distribution of power along ψ and θ for radiation from a 15-T, 15-period wiggler on a 6-GeV storage ring (100 mA).

Peak Surface Power Density:

$$W_{xy}(W/mm^2) = P_{xy}/\ell^2(m^2). \tag{36}$$

In the above discussion we have not considered the following:

1. The spread in the angular distribution with photon energy.

2. Spatial and angular spreads in the positron beam in the ring.

3. The effect of finite length of the wiggler source.

The above factors do not have significant influence other than to produce some smearing of the distribution. At distances large compared to wiggler length ($\ell >> L$, a normal condition at the 6-GeV source), the effect of finite wiggler length is not important.

In Table 6, the parameters related to the above discussion are used to compare various planned wigglers, including the 1.5-T wiggler for the 6-GeV storage ring. The peak power per unit solid angle delivered by this wiggler is an order of magnitude larger than that for the superconducting wiggler (X-17) on the NSLS. On the other hand, the total power of the 1.5-T (6-GeV) design is 5 times smaller than for the X-17 (NSLS) device.

B. Flux and Brilliance of Wigglers

It is important to choose the parameters for the 6-GeV wiggler and compare the resulting spectral characteristics with those of wigglers on existing synchrotron sources. We have selected 3 wiggler-type devices of which two are multipole wigglers and one is an energy shifter.

In Table 7 we present the parameters used in the calculation of the spectral characteristics for various wigglers. In Figs. 22 and 23, the flux and brilliance observed along the axis of the three 6-GeV wigglers are presented. In Figs. 24 and 25, the flux and brilliance along the wiggler axes of two multipole wigglers on a 6-GeV storage ring are compared with those of devices on presently operating synchrotrons.

We wish to draw attention to the fact that the values of the critical energies in Table 7 are for a normal observation angle ($\theta = 0$) along the wiggler axis. The critical energy decreases for non-zero values of the observation angle θ [9].

C. Angular Apertures for Wiggler Ports

The opening of the beam port has to be properly designed to collect the wiggler radiation without any obstruction. The angular aperture in the horizontal plane is given by

$$\theta_x = \frac{2K}{\gamma} + 2\left(\frac{1}{\gamma^2} + \sigma_x'^2\right)^{1/2}. \tag{37}$$

Table 6. Comparison of Planned Wigglers on Various Sources

Parameters	SSRL Beamline VIII	NSLS X-17	6-GeV 1.5-T
Energy (GeV	3.0	2.5	6.5
Current (mA)	100	500	100
B_o (T)	1.3	6.0*	1.5
ρ (m)	7.8	1.39	13.3
Number of Poles	30	6	30
λ_o (cm)	12.85	17.4	10.0
E_c (keV)	7.8	24.9	35.9
K	15.6	97.5	14.0
Flux at E_c ($x10^{14}$)	1.4	0.24	2.9
2ψ (mrad)	0.41	0.49	0.2
2θ (mrad)	5.3	39.9	2.4
Total Power (kW)	1.85	37.9	7.7
Distance from the Source, ℓ (m)	10	10	50
Beam Width 2θ at ℓ (m)	53.0	400.0	120.0
Beam Height 2ψ at ℓ (m)	4.1	4.9	10.0
P_x (W/mrad)	456	1218	4209
P_{xy}(W/mrad^2)	700	3782	31376
W_x(W/mm) at ℓ (m)	46	122	84
W_{xy}(W/mm^2) at ℓ (m)	17	38	13

*Actual design consists of 5 poles with 6 T and 2 poles with 2 T.

Table 7. Parameters for Various Transverse Wiggler Sources

	6-GeV WIGI	6-GeV WIGII	6-GeV WIGIII	CHESS 6-Pole	SSRL VIII	SSRL VI	NSLS X-17
E_R (GeV)	6.0	6.0	6.0	5.5	3.0	3.0	2.5
I (mA)	100	100	100	40	100	100	500
ρ (m)	6.67	16.7	28.6	13.2	7.69	8.36	1.39
B_o (T)	3.0	1.2	0.7	1.39	1.3	1.2	6
σ_x (mm)	0.1	0.1	0.1	1.9	2.5	3.2	0.3
σ_y (mm)	0.03	0.03	0.3	1.2	0.15	0.15	0.02
σ_x' (mrad)	0.073	0.073	0.073		0.18	0.18	0.24
σ_y' (mrad)	0.024	0.024	0.024	0.05	0.03	0.03	0.04
E_c (keV)	71.8	28.7	16.8	27.9	7.78	7.16	24.9
Number of Poles	3	20	30	6	30	54	6
Period, λ_o (cm)	15	20	10	35	12.85	7.25	17.8
K	42	22	17	45	15.6	8.1	99.8
L (m)	0.225	2.0	1.5	1.05	1.93	1.96	0.53
Total Power (kW)	4.6	6.5	1.7	1.6	1.85	1.6	37.9

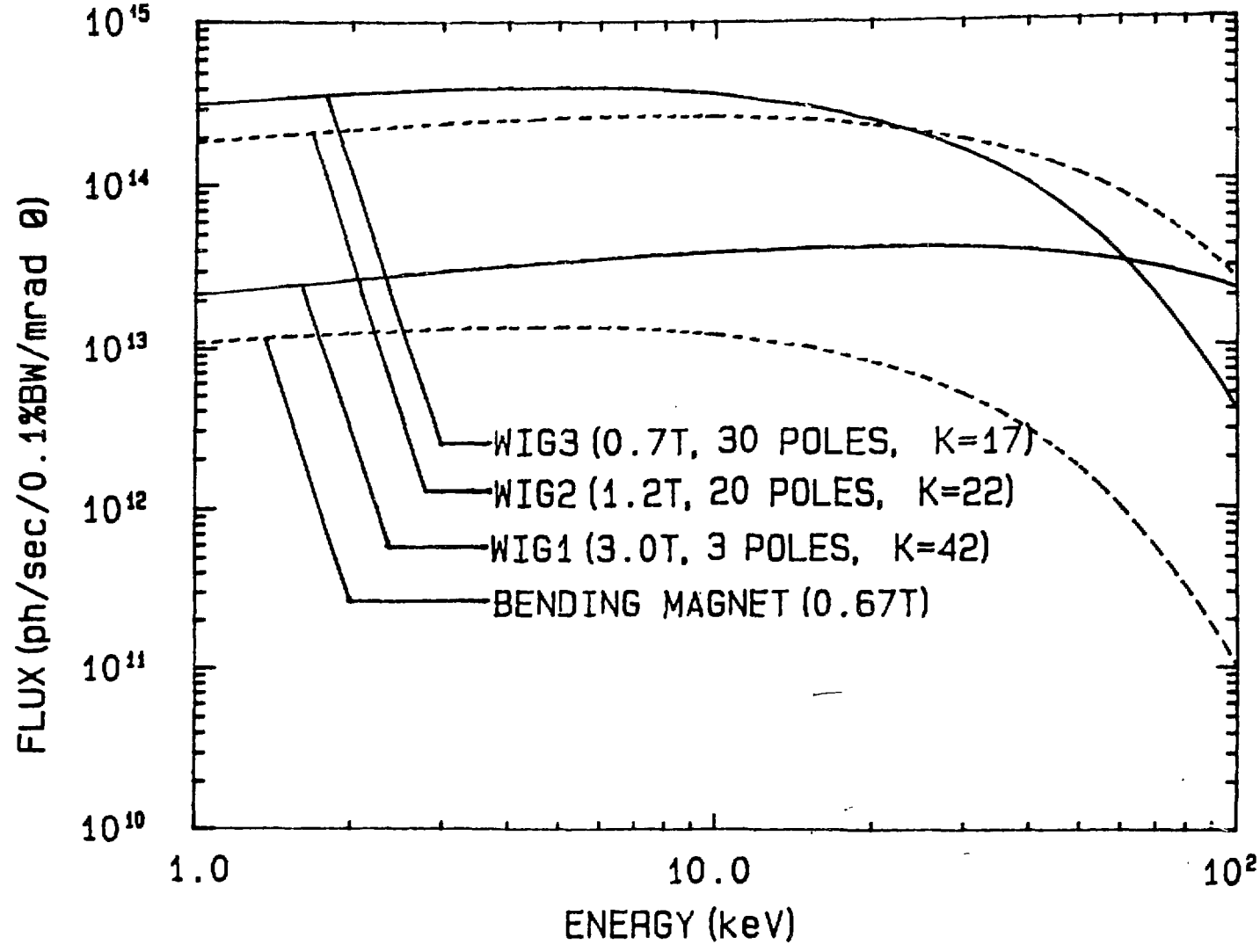

Fig. 22. Flux from wigglers on a 6-GeV storage ring, (100 mA), compared with that from a bending magnet.

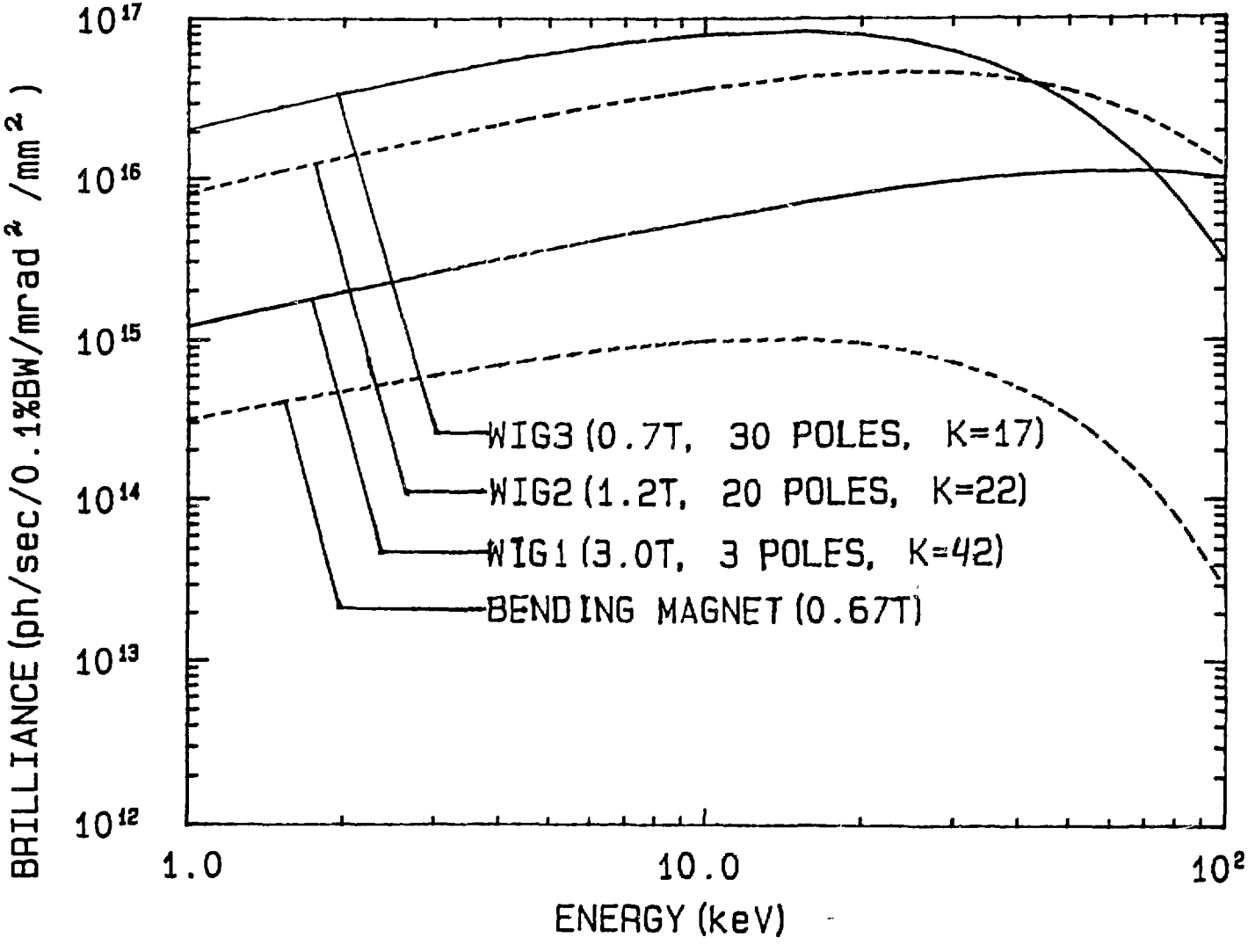

Fig. 23. Brilliance of radiation from wigglers on a 6-GeV storage ring (100 mA).

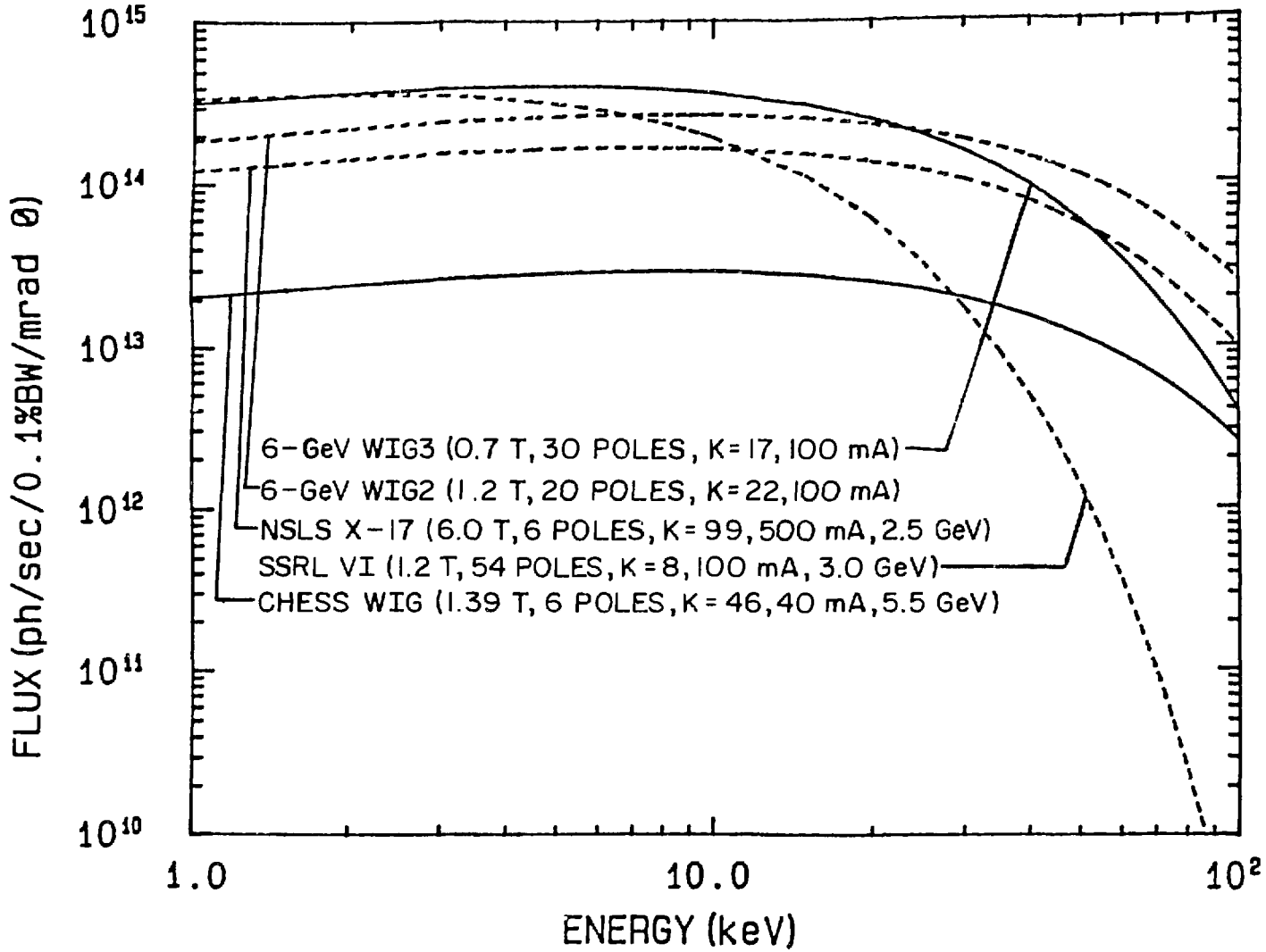

Fig. 24. Flux from wigglers on a 6-GeV storage ring, compared with those from wigglers on other synchrotron sources.

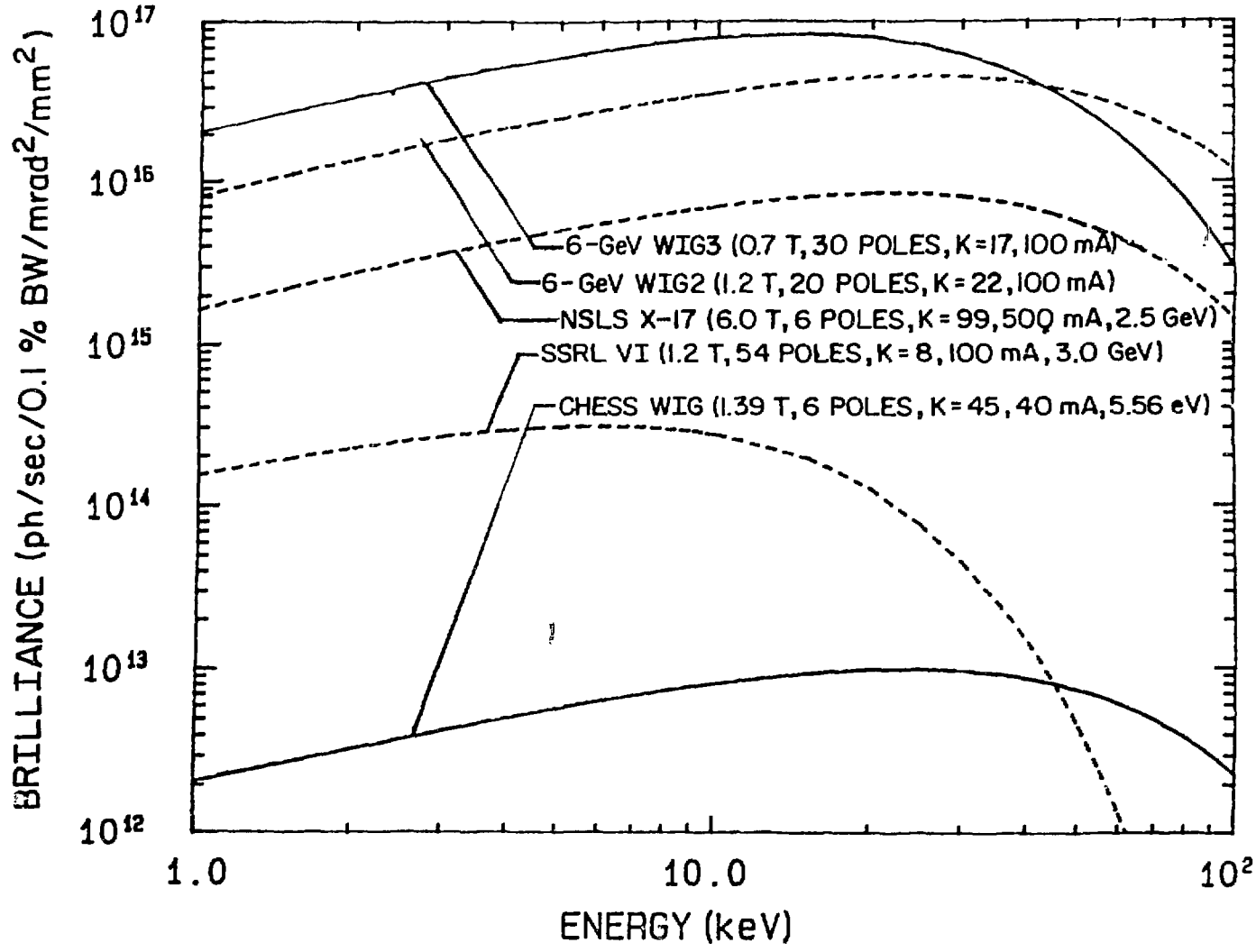

Fig. 25. Brilliance from wigglers on a 6-GeV storage ring, compared with those from wigglers on other synchrotron sources.

For the 6-GeV lattice, because of the low emittance and low β values,

$$\theta_x \approx \frac{2K}{\gamma} .$$

Similarly, the angular aperture in the vertical plane is represented by

$$\theta_y = 2\left(\frac{1}{\gamma^2} + \sigma_y'^2\right)^{1/2} . \qquad (38)$$

Again, for the wiggler insertion with a low β_y value (see Table 2),

$$\theta_y \approx \frac{2}{\gamma} .$$

Because of smaller values of θ_x and θ_y for the wigglers on a 6-GeV storage ring compared with those on lower GeV sources, the front-end design should be straightforward.

D. Wiggler Polarization

The positron beam through a wiggler experiences bending forces in the opposite direction. Hence, the radiation is linearly polarized only in the orbital plane (xz). Away from this plane we have polarizations of opposite helicity from successive poles of the wiggler, which add to destroy the net polarization, except for the residual linear component. This should be contrasted with the situation for a BM and a single-pole wiggler (Energy Shifter), where away from the orbital plane one has elliptically polarized radiation (section IV.A).

E. Low-E_c/High-Brilliance Wigglers

In utilizing radiation from a BM, undulator, or wiggler source in low-energy applications (from 3 to 8 keV), the contribution from higher harmonics through a monochromator is hard to avoid on a 6-GeV storage ring. The critical energy of the BM radiation is 16 keV and those of wigglers discussed thus far are even higher. Even if the undulator first harmonic is tuned to the desired energy, the monochromator will pass some of the higher (even and odd) harmonics (depending on the value of K). A normal procedure to reduce the higher harmonics is to detune a two-crystal monochromator up to 50%, which also results in a net loss of photon flux. In the following we suggest a design for a wiggler with low critical energy which can reduce the contributions from the higher harmonics. This also enhances the flux and the brilliance.

The design involves the use of low-field wiggler magnets (with B_o less than that of the BM field, 0.67 T) in the straight section with long periods (λ_o) so that K can be of the order of 10.

In Table 8, we present parameters for two such wigglers. The plot of flux vs energy for these devices is compared with that of BM radiation in Fig. 26.

Table 8. Parameters for Low-E_c Wigglers on a 6-GeV Storage Ring (100 mA)

	WIG IV	WIG V
B_o (T)	0.1	0.2
ρ (m)	200	100
E_c (keV)	2.4	4.8
Number of Poles	6	10
Period, λ_o (cm)	83	50
K	7.8	9.3
L (m)	4.98	5
Total Power (W)	57	227
Flux at E_c ($x10^{13}$)	5.8	9.6

VII. TIME STRUCTURE OF 6-GeV STORAGE RING

The use of the time structure of synchrotrons has been demonstrated in the study of dynamic phenomena in chemical, physical and biological systems. Because of the very high brilliance of the 6-GeV source, temporal studies are even more justified. In general, the bunch lengths can be from a fraction of a picosecond to several nanoseconds. The storage ring can contain a single bunch or several. If there is only one bunch, once the system to be investigated is excited by the initial pulse, one then has an interval of 2.67 μsec before the next bunch arrives. One can also study a system at any time over a 2.67-μsec period for the duration of the bunch if the system is excited by another (e.g., laser) source. If most users are not interested in this 'time mode', a multibunch mode is preferable for general operation. In that case, a single-bunch operation can be simulated through the use of a WOBLER which sorts one bunch from the rest at one port on the ring. Such a device will deliver radiation from a single bunch at one port although all the bunches are present in the ring. The duration of the bunch on the 6-GeV storage ring is expected to be about 1000 psec. The exact value will be decided with user input to the storage-ring designers. If this duration has to be reduced considerably, then the storage ring will have a lower current.

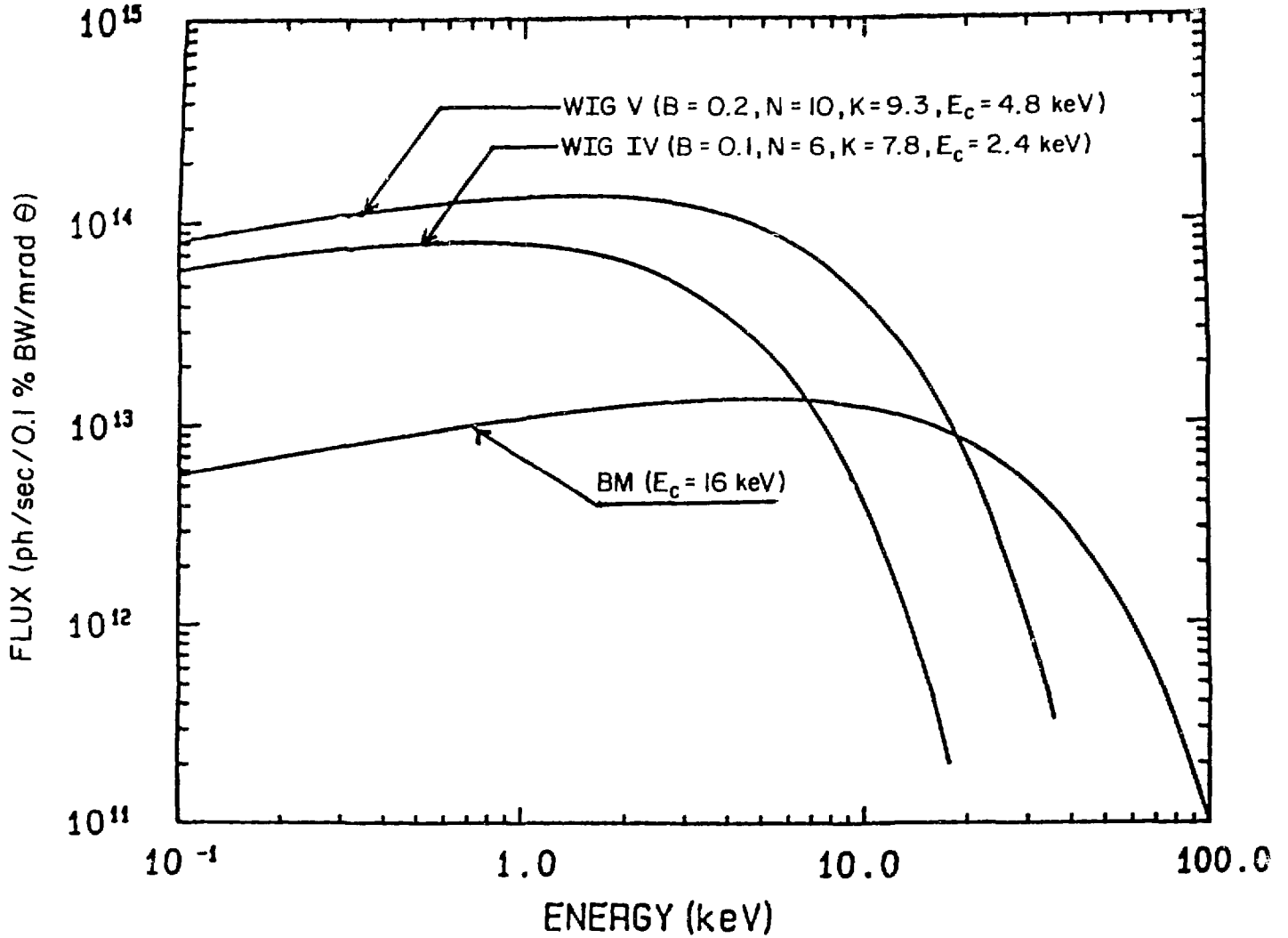

Fig. 26. Flux from low-E_c wigglers useful for harmonics-free low-energy operation on a 6-GeV storage ring (100 mA).

In Table 9 we present information on the time structure of various synchrotron orbits. Many types of experiments will be done in the future. These include diffraction, absorption, topography, stroboscopic imaging, and time development of systems.

Table 9. Time Structure of Various Storage Rings

	SSRL	CHESS	NSLS	6-GEV
E_c(keV)	4.7	8.7	5.0	16.0
Orbit Period (nsec)	760	2560	568	2670
Number of Bunches*	1(4)	1(7)	30	1(10)
Bunch Duration (psec)	300	160	1700	1000
Interpulse Period* (nsec)	760(190)	2560(366)	18.9	267(26.7)

*Numbers in ( ) refer to alternative mode of operation.

VIII. DISTRIBUTION OF INSERTION DEVICES ON A 6-GeV STORAGE RING [10]

For those who are involved in ring design, information on the distribution of insertion devices is essential for the optimization of a lattice. Users, on the other hand, would like to postpone this issue as much as possible so that insertion devices based on developing technologies can be built to tackle scientific research areas which are just emerging or not yet conceived. Since the project planning process should continue, the users must present a plan based on current needs and the storage ring designers must build enough flexibility into the lattice so that the design can easily accommodate newer insertion devices.

On a 6-GeV storage ring, the most common types of sources will be BMs, multipole wigglers, energy shifters, and undulators. There will be, in addition, more complex devices such as crossed undulators, devices with variable K to transform them from an undulator to a wiggler regime ($0.4 \leq K \leq 20$), extra-long undulators (10-18 m), undulators with flat-top energy peaks [11], WOBLERS for timing experiments, etc. The issue of types of devices should be addressed in future 6-GeV workshops.

In this section we will orient the reader to the details of the lattice and to the nature of the experimental stations. In Fig. 27 a part of the lattice is shown, along with various types of experimental stations.

The BM radiation will be delivered to users at 32 of the 64 bending magnets. It is easy to split the beam into at least two parts of 6 mrad each, to be delivered to two BM experimental stations.

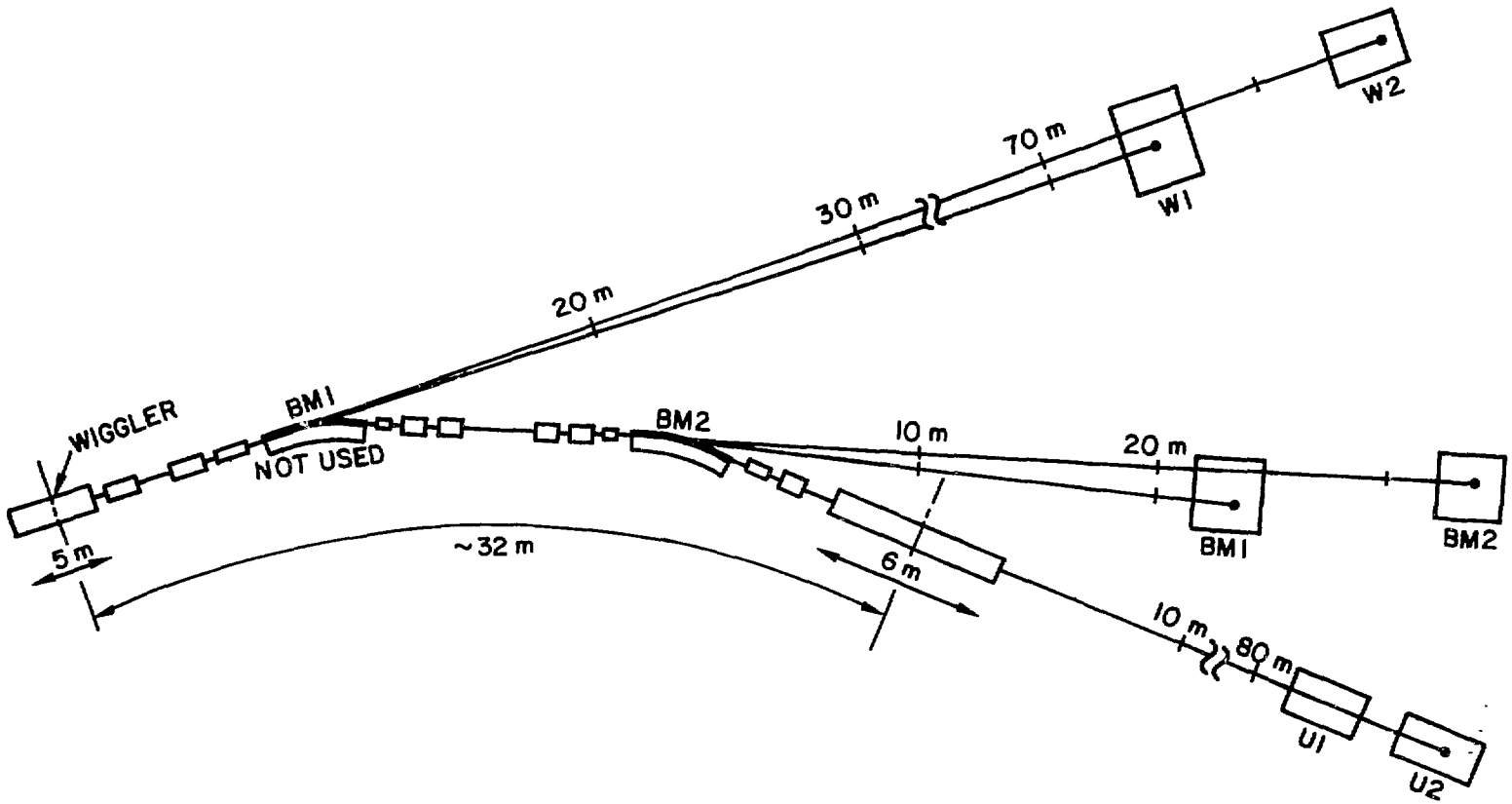

Fig. 27. A typical layout of beam lines and experimental stations on various radiation sources on a 6-GeV storage ring. The lattice of the storage ring shown has no relevance to exact design.

Out of 32 straight sections, 28 will be available for insertion devices. The distribution of wigglers and undulators in these 28 slots will have to satisfy certain symmetry considerations for the proper operation of the storage ring. For the energy shifters and multipole wigglers, the horizontal spread of the beam is 3 to 8 mrad, depending on the K value of the device. This beam can be split into two and delivered to two wiggler experimental stations simultaneously. The undulator sources have a limited divergence and they cannot be split with ease. Hence, they are expected to serve only one experimental station at any given time. At the undulator straight sections, we can expect to have a set of undulators (with different length of periods) available on a carousel.

As an example, we can estimate the total possible experimental stations on the 6-GeV storage ring by distributing 22 undulators and 6 wigglers in the straight sections (2 undulator and 2 wiggler straights are for storage ring components):

BMs:	32 x 2 = 64	experimental stations
Energy shifters + multipole wigglers:	6 x 2 = 12	experimental stations
Undulators:	22 x 2 = 44	tandem stations
Total:	120	stations

The above numbers are only given to project the magnitude of the 6-GeV facility. The emphasis during the early years of commissioning will naturally be on the insertion devices, primarily the undulators.

ACKNOWLEDGMENTS

We would like to thank Y. Cho, F. Y. Fradin, K. L. Kliewer, S. Krinsky, and D. Moncton for their input in the preparation of this document.

REFERENCES

1. Y. Cho, Argonne National Laboratory, unpublished report (LS-31), 1985.*
2. For example, see C. Kunz, Synchrotron Radiation (Springer, New York, 1979).
3. S. Krinsky et al., BNL Rept. 31989, Sept. 1982.
   S. H. Kim, Argonne National Laboratory, unpublished reports (LS-7, -8 and -29), 1985.
   R. Coisson, ESRP-IRM-34/84, -84/84.
   K. Halbach, Nucl. Instrum. Meth. 187 (1981) 109.
   G. K. Shenoy, Argonne National Laboratory, unpublished reports (LS-22 and -24), 1985.
4. S. Bartalucci, ESRP-IRM-68/84.
   A. Luccio, ESRP-IRM-12/84.
5. H. Kitamura, Jpn. J. Appl. Phys. 19 (1980) L185.

*All cited LS documents are available from Argonne National Laboratory.

6. B. Kincaid, J. Appl. Phys. 38 (1977) 2684; J. Opt. Soc. Am. B2 (1985) 1294.
7. K.-J. Kim, LBL Rept. 18313, May 1984.
8. R. T. Avery, Nucl. Instrum. Meth. 222 (1984) 146.
9. G. K. Shenoy and P. J. Viccaro, Argonne National Laboratory, unpublished results, 1985.
10. G. K. Shenoy, Argonne National Laboratory, unpublished results, 1985.
11. G. K. Shenoy and P. J. Viccaro, Argonne National Laboratory, in preparation.

Distribution for ANL-85-69

Internal:

M. B. Brodsky
Y. Cho
D. R. Diercks
W. A. Ellingson
F. Y. Fradin
B.R.T. Frost
D. Gruen
K. L. Kliewer
G. K. Shenoy (320)
E. M. Stefanski
L. Teng
R. W. Weeks
H. Wiedersich
ANL Patent Dept.
ANL Contract File
ANL Libraries
TIS Files (6)

External:

DOE-TIC, for distribution per UC-28 (96)

DOE Chicago Operations Office:

Manager
D. L. Bray
F. Herbaty
V. H. Hummel

The University of Chicago:

N. M. O'Fallon

Materials Science and Technology Division Review Committee:

C. B. Alcock, U. Toronto
A. Arrott, Simon Fraser U.
R. C. Dynes, Bell Labs., Murray Hill
A. G. Evans, U. California, Berkeley
H. K. Forsen, Bechtel National, Inc., San Francisco
E. Kay, IBM San Jose Research Lab.
M. B. Maple, U. California, San Diego
P. G. Shewmon, Ohio State U.
J. K. Tien, Columbia U.
J. W. Wilkins, Cornell U.

Office of Basic Energy Sciences:

R. J. Gottschall
L. Ianniello
T. Kitchens
F. V. Nolfi
D. Stevens
M. Wittels